

Supplementary Materials for

A cargo-sorting DNA robot

Anupama J. Thubagere, Wei Li, Robert F. Johnson, Zibo Chen,
Shayan Doroudi, Yae Lim Lee, Gregory Izatt, Sarah Wittman,
Niranjan Srinivas, Damien Woods, Erik Winfree, Lulu Qian*

*Corresponding author. Email: luluqian@caltech.edu

Published 15 September 2017, *Science* **357**, eaan6558 (2017)
DOI: 10.1126/aan6558

This PDF file includes:

Materials and Methods
Supplementary Text
Figs. S1 to S14
Tables S1 and S2
References

Supplementary Materials for A cargo-sorting DNA robot

Anupama J. Thubagere, Wei Li, Robert F. Johnson,
Zibo Chen, Shayan Doroudi, Yae Lim Lee, Gregory Izatt, Sarah Wittman,
Niranjan Srinivas, Damien Woods, Erik Winfree & Lulu Qian*

*correspondence to: luluqian@caltech.edu

Contents

1 Materials and methods	2
1.1 DNA oligonucleotide synthesis	2
1.2 Annealing protocol and buffer condition	2
1.3 Purification	2
1.4 DNA origami concentration measurement	2
1.5 Fluorescence spectroscopy	2
1.6 Atomic force microscopy	3
2 Supplementary data and analysis	4
2.1 The rigidity of DNA origami affects the undesired reactions	4
2.2 The DNA sequence of the foot domains of the robot affects the rate of walking	5
2.3 A biophysical model of the walking mechanism	6
2.4 The purity of DNA origami affects the completion level of desired reactions	10
2.5 Numerical analysis of the random walk	11
2.6 Cargo pick-up	12
2.7 Procedure for preparing cargo-sorting samples	13
2.8 Negative control for cargo sorting without a robot	14
2.9 Procedure for preparing cargo-sorting samples for AFM imaging	15
2.10 AFM images of the cargos at their initial locations and destinations	16
2.11 Cargo sorting with mixed populations of DNA origami	17
2.12 Analysis of the completion levels in the cargo-sorting experiments	18
2.13 Multiple robots collectively performing a cargo-sorting task	19
3 Cadnano diagram	20
3.1 Double-layer square DNA origami design	20
4 DNA sequences	21
4.1 Staples	21
4.2 Robot, track, cargo and goal strands	25
References	26

1 Materials and methods

1.1 DNA oligonucleotide synthesis

DNA oligonucleotides were purchased from Integrated DNA Technologies (IDT). The regular staples, track staples and trigger strands were purchased unpurified (standard desalting). The robot, cargo and goal strands, the inhibitor strands, and the staples with extensions for localizing robot, cargos and goals (referred to as robot start, cargo and goal staples, respectively) were purchased purified (HPLC). All strands were purchased at 100 μM in TE buffer, pH 8.0, and stored at 4 °C.

1.2 Annealing protocol and buffer condition

DNA origami was annealed with 30 nM M13 scaffold (Bayou Biolabs), a 10-fold excess of the regular, track, robot start, cargo and goal staples, 11-fold excess of the cargo attacher strands, and 12-fold excess of the cargo strands in 1 \times TAE buffer with 12.5 mM Mg²⁺. The buffer was prepared from 50 \times TAE, pH 8.0 (Fisher BioReagents) and magnesium acetate tetrahydrate (Fisher BioReagents). The inhibited robot and goal complexes were annealed at 20 μM with a 20% excess of the inhibitor strands. Annealing was performed in a thermal cycler (Eppendorf), first heating up to 90 °C for 5 minutes, and then slowly cooling down to 20 °C at the rate of 6 sec per 0.1 °C.

1.3 Purification

After annealing, the DNA origami sample was loaded on a 2% agarose gel, run on ice for 2 hours at 80 V in 1 \times TAE/Mg²⁺ buffer. The appropriate bands were then cut out from the gel and purified using the Freeze 'N Squeeze DNA gel extraction spin columns (Biorad). The inhibited robot and goal complexes were purified using 15% polyacrylamide gel electrophoresis (PAGE). After incubating the DNA origami with an approximately 2-fold excess of the inhibited robot and goal complexes for 5 hours at room temperature, the sample was purified three times using 0.5 mL and 100 KDa spin filters (Amicon, #UFC510096), each time for 12 minutes at 2,500 Relative Centrifugal Force (RCF).

1.4 DNA origami concentration measurement

The concentration of DNA origami with the robot, tracks, cargos and goals was measured in a spectrofluorimeter (Fluorolog-3, Horiba), using the fluorescence signal of an embedded staple labeled with a ROX fluorophore, and comparing the signal with a calibration curve (i.e. a linear fit of the measurements of raw fluorescence levels at varying concentrations) of the fluorophore-labeled strand by itself.

1.5 Fluorescence spectroscopy

Fluorescence kinetics data were collected every 2 minutes in a spectrofluorimeter (Fluorolog-3, Horiba). Experiments were performed with 50 μL reaction mixture per cuvette, in fluorescence cuvettes (Hellma #105.251-QS) at 25 °C. The excitation/emission wavelengths were set to 534/554 nm for ATTO 532 and 602/624 nm for ATTO 590. Both excitation and emission bandwidths were set to 5 nm, and the integration time was 10 seconds for all experiments. Samples for fluorescence spectroscopy were diluted to 3 nM of the origami concentration. Baseline measurements of the samples were taken for 30 minutes. A 20-fold

excess of the trigger strands was then added. To measure the maximum possible completion level at the end of each experiment, a 20-fold excess of free-floating robot strands with and without quenchers was added in random walk and cargo pick-up experiments, respectively; a 20-fold excess of free-floating goal strands with quenchers was added in cargo sorting experiments.

1.6 Atomic force microscopy

Samples for AFM imaging were prepared by diluting the origami to 1 nM in 1× TAE/Mg²⁺ buffer. After dilution, 40 μ L of the sample was deposited onto freshly cleaved mica (SPI Supplies, 9.5 mm diameter, #01873-CA). After 3 minutes the solution was removed and 40 μ L of 1× TE/Mg²⁺ buffer was added onto the mica, then the sample was imaged. Samples of cargo-sorting experiments were first incubated with a 20-fold excess of goal remover strands for one hour at room temperature, and then incubated with 10 units per μ L of exonuclease I (New England Biolabs #M0293S) for 18 hours at 25 °C before imaging. AFM images were taken in tapping mode in fluid on a Dimension FastScan Bio (Bruker) using FastScan-D probes (Bruker). All images were scanned at a resolution of 1024 lines with 1024 pixels per line.

2 Supplementary data and analysis

2.1 The rigidity of DNA origami affects the undesired reactions

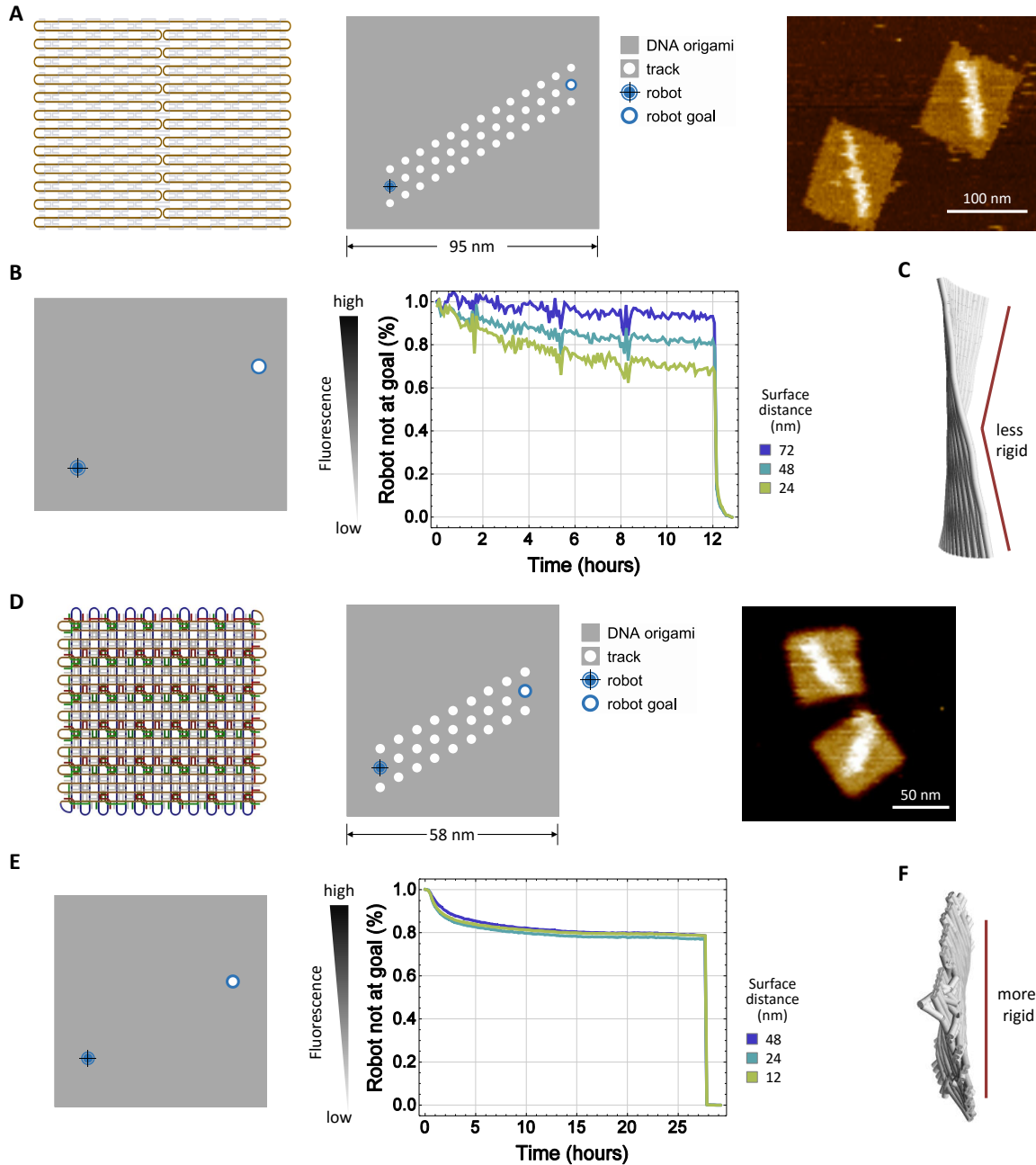


Fig. S1. The rigidity of DNA origami affects the undesired reactions. (A) Scaffold path, schematic diagram, and Atomic Force Microscope (AFM) image of a single-layer rectangular DNA origami (6) with a linear track. (B) Schematic diagram and fluorescence kinetics data of a negative control experiment for the robot reaching the goal without any track on the single-layer origami. Three distinct surface distances between the robot and the goal were tested. (C) CanDo (32) diagram showing the predicted deformations of the single-layer origami structure. Substantial thermal fluctuations can be observed in a CanDo movie. (D) Scaffold path, schematic diagram, and AFM image of a double-layer square DNA origami with a linear track. (E) Schematic diagram and fluorescence kinetics data of a negative control experiment for the robot reaching the goal without any track on the double-layer origami. Three distinct surface distances between the robot and the goal were tested. (F) CanDo diagram showing the degree of thermal fluctuations of the double-layer origami structure. Limited thermal fluctuations can be observed in a CanDo movie.

2.2 The DNA sequence of the foot domains of the robot affects the rate of walking

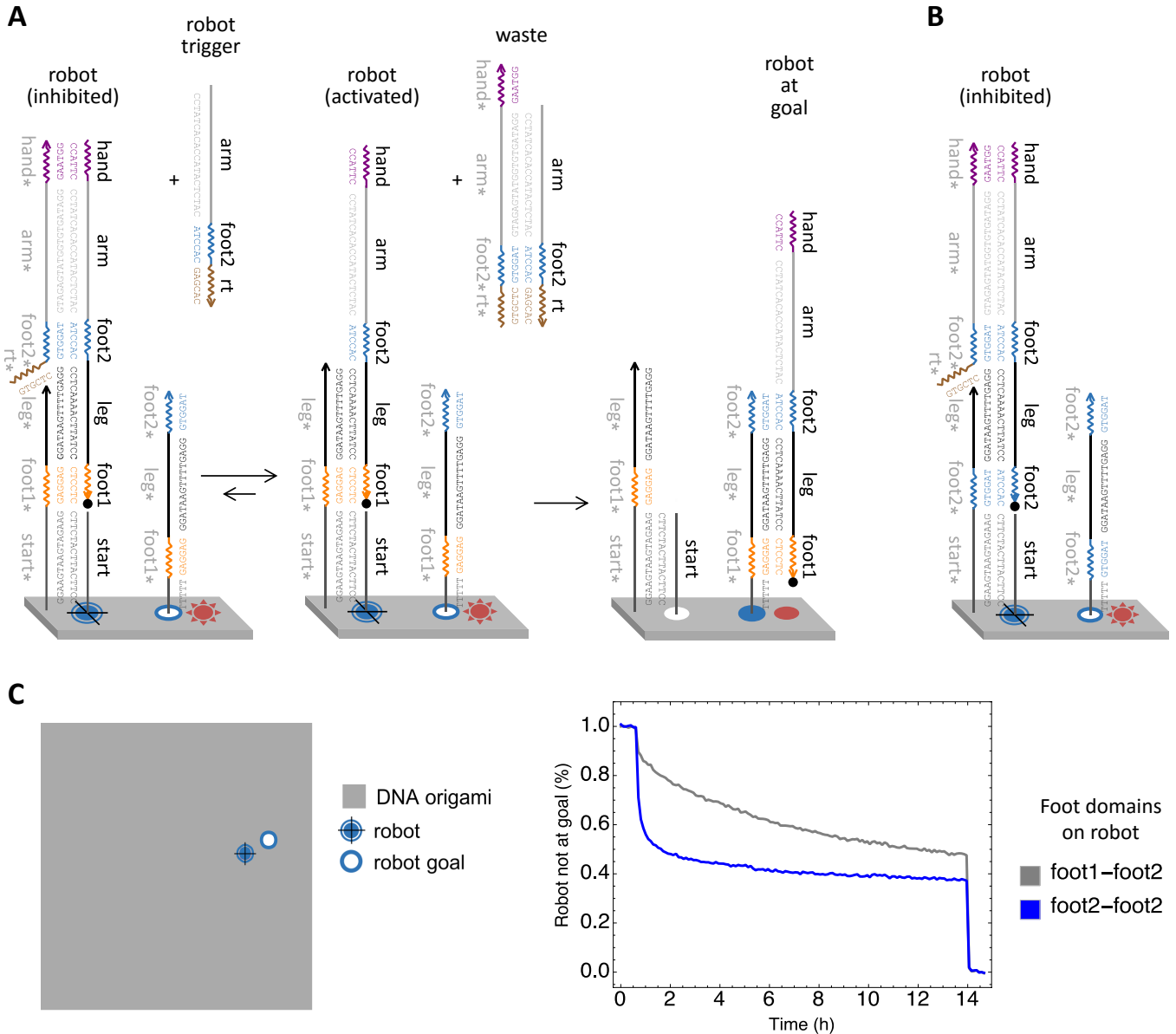


Fig. S2. The DNA sequence of the foot domains of the robot affects the rate of walking. (A) Sequence-level diagram of the mechanism of the robot making a single step to reach the goal after being triggered. Two distinct sequences are used for the two feet. (B) Sequence-level diagram of the same setup as shown in A, but with identical sequences used for the two feet. (C) Schematic diagram and fluorescence kinetics data of the robot taking a single step. Two sequence choices shown in A and B were both tested. The sequence of foot1 has a stronger standard free energy and that of foot2 has a weaker standard free energy. NUPACK (52) predicts -8.76 kcal/mol for foot1 and -8.55 kcal/mol for foot2 at 25 °C, without considering the stacking energy on the 5' and 3' ends.

2.3 A biophysical model of the walking mechanism

To better understand the mechanism of walking, we developed a biophysical model. We do not have enough experimental data to accurately fit parameters or verify mechanisms involved in the model, but it is already conceptually insightful for understanding why the robot walks at a fairly slow rate and how the rate could potentially be much faster.

We start with an irreversible reaction from track type 1 to the goal, as shown in Fig. S3A. In this model, RTr1[27] is the robot at the track1 location. 27 corresponds to the total number of nucleotides in the robot strand that are involved in walking: two foot domains that each have 6 nucleotides and one leg domain that has 15 nucleotides. RG[i] is the robot with i nucleotides bound to the goal location. k_h is the rate constant of localized hybridization. In position i , k_{5d}^i and k_{3d}^i are the rate constants of disassociation from the 5' end and 3' end of the robot strand, respectively. k_{5b}^i and k_{3b}^i are the rate constants of a single-base-pair branch migration step from the i -th nucleotide toward the 5' end and 3' end of the robot strand, respectively.

k_h can be estimated using two methods. First, similar to the estimates in localized DNA circuits (50, 53), $k_h = \text{the rate constant of hybridization in solution} \times \text{the local concentration}$. The rate of DNA hybridization is approximately $10^6 / \text{M/s}$ at 25°C (54). The local concentration can be estimated as $(1 / N_A) / (4\pi/3 \times (6 \text{ nm})^3)$, where N_A is the Avogadro's constant, and 6 nm is the distance between the robot start and goal locations. Therefore, $k_h \approx 1835 / \text{s}$. Second, k_h can be estimated as the rate constant of closing a hairpin. From a previous study on the kinetics of hairpin opening and closing (55), $k_{close}^n \approx k_0(n + 5)^{-2.5}$ at 25°C , where n is the loop size, and $k_{close}^{30} \approx 5 \times 10^3 / \text{s}$. In our system, the loop size can be estimated as $((15 + 6 + 15) \text{ bp} \times 0.34 \text{ nm/bp} + 6 \text{ nm} + (15 + 6) \text{ nt} \times 0.43 \text{ nm/nt}) / (0.43 \text{ nm/nt}) = 63 \text{ nt}$. Therefore, $k_h \approx 950 / \text{s}$. We use $k_h = 10^3 / \text{s}$, which roughly agrees with both estimates.

For a generic sequence, the disassociation rate constant can be modeled as $k_d = 10^{(6-L)} / \text{s}$ for a hybridization domain of length L with a reference standard free energy $\overline{\Delta G}$ for each base pair, which is close to the average standard free energy at 25°C (54). Therefore, in our system, $k_{5d}^i = 10^{6-i} / \text{s}$ and $k_{3d}^i = 10^{6-(27-i)} / \text{s}$. Because we are interested in how the standard free energy of the foot domain near the 3' end of the robot strand affects the rate of walking (Fig. S2), for the irreversible reaction shown in Fig. S3A, we re-define $k_{3d}^i = 10^{6-\Delta G/\overline{\Delta G}(27-i)} / \text{s}$, where ΔG is the standard free energy for each base pair with a specific sequence that could be stronger ($\Delta G/\overline{\Delta G} > 1$) or weaker ($\Delta G/\overline{\Delta G} < 1$) than average.

From a previous biophysics study of strand displacement reactions (56), the initiation of branch migration is about $5 / \text{s}$ and each of the following steps is about $10^4 / \text{s}$. We use these two rate constants to define k_{5b}^i , for branch migration away from the DNA origami surface (except there will be no initiation step for an irreversible reaction that ends at the 5' end). However, taking the elasticity of double- and single-stranded DNA into consideration (34), branch migration toward the DNA origami surface should lead to a tighter stretch of the DNA strands and thus a slowdown of the rate constant. Since we designed appropriate linker lengths for the robot to reach an adjacent track location (Fig. S4A), the strands should not be overstretched and thus should remain within the “entropic elasticity” regime where the force increases linearly with the distance stretched, corresponding to a quadratic energy cost for stretching the “entropic spring”. Thus we define $k_{3b}^i = 5 / \text{s}$ when $i = 6$, $k_{3b}^i = 10^4 / \text{s}$ when $6 < i \leq th$, and $k_{3b}^i = 10^{4-w(i-th)} / \text{s}$ when $i > th$, where th is nucleotide location for which the force starts to increase when branch migration moves close enough to the origami surface, and w is the energy change per step. This model is qualitatively consistent with a molecular dynamics study of a similar system (33).

By comparing simulation with the experimental data shown in Fig. S2C, we were able to determine that $th = 19$ and $w = 2$ are reasonable parameters for our system. The model suggest that (1) the entropic cost of stretching the DNA strands significantly slows down branch migration toward the DNA origami

surface, when the junction of branch migration is close enough to the surface. (2) Branch migration becomes slower than disassociation near the end of the reaction, resulting in disassociation prior to branch migration through the foot domain. Thus, a weaker sequence of the foot domain near the 3' end of the robot leads to a faster overall reaction rate because of faster disassociation. (3) A small difference in the standard free energy of the DNA sequence ($\Delta G/\overline{\Delta G} = 1.1$ vs. 0.8 for each base pair) can result in a large difference in the rate of the robot taking a single step (half completion time ≈ 15 hours vs. 10 minutes).

Similarly, a reversible strand displacement reaction of the robot walking from one track location to another ($RTr1[27] \rightleftharpoons RTr2[27]$) can be modeled with analogous hybridization, branch migration and disassociation steps (Fig. S3B). The disassociation rate constants are the same as discussed above:

$$k_{5d}^i = 10^{6-i} /s$$

$$k_{3d}^i = 10^{6-(2T+15-i)} /s$$

Branch migration toward and away from the origami surface now both include an initiation step. To explore how the rate of initiation and the strength of the foot domains affect the overall speed of walking, we set the initiation rate constant to be a variable k_0 , and the length of the foot domains in the robot strand to be a variable T , while keeping the track strands unchanged:

$$k_{5b}^i = \begin{cases} 10^4 /s & i < T + 15 \\ k_0 & i = T + 15 \end{cases}$$

$$k_{3b}^i = \begin{cases} k_0 & i = T \\ 10^4 /s & T < i \leq th - 6 + T \\ 10^{4-w(i-(th-6+T))} /s & i > th - 6 + T \end{cases}$$

The energies of the beginning and end states shown in Fig. S3B should be approximately the same, as in both cases the robot is bound to its track by the same total number of base pairs and has similar geometric constraints. To satisfy detailed balance, the ratio between the product of all forward rate constants and that of all reverse rate constants for all pathways between any two given states should also be the same. Using these two requirements, all hybridization rate constants can be calculated based on k_{5h}^T and the disassociation and branch migration rate constants:

$$k_{5h}^i = \begin{cases} 10^3 /s & i = T \\ \frac{k_{5h}^T \prod_{n=T}^{i-1} k_{3b}^n}{k_{5d}^T \prod_{n=T+1}^i k_{5b}^n} \times k_{5d}^i /s & i > T \end{cases}$$

$$k_{3h}^i = \begin{cases} \frac{k_{3h}^{T+15} \prod_{n=i+1}^{T+15} k_{5b}^n}{k_{3d}^{T+15} \prod_{n=i}^{T+14} k_{3b}^n} \times k_{3d}^i /s & i < T + 15 \\ 10^{3-\sum_{n=1}^{20-th} n \times w} /s & i = T + 15 \end{cases}$$

Before the initiation of branch migration (k_0) becomes the rate limiting step, the overall reaction rate will still largely depend on the disassociation near the end of the reaction, and therefore the robot walks

at a fairly slow rate of roughly 5 min per step. Since the critical difference between the first and second step of branch migration is the presence of one versus two single-stranded tails at the branch point (56), k_0 could potentially be increased from 5 /s to at least 10^3 /s by adding a few Ts at the 3' end of the track strands. Simulations suggest that, with an increased k_0 , weaker foot domains (e.g. 2 to 4 nucleotides) could speed up walking by at least tens to hundreds of times (Fig. S3B).

The biophysics of the DNA robot performing random walking merits further theoretical and experimental study.

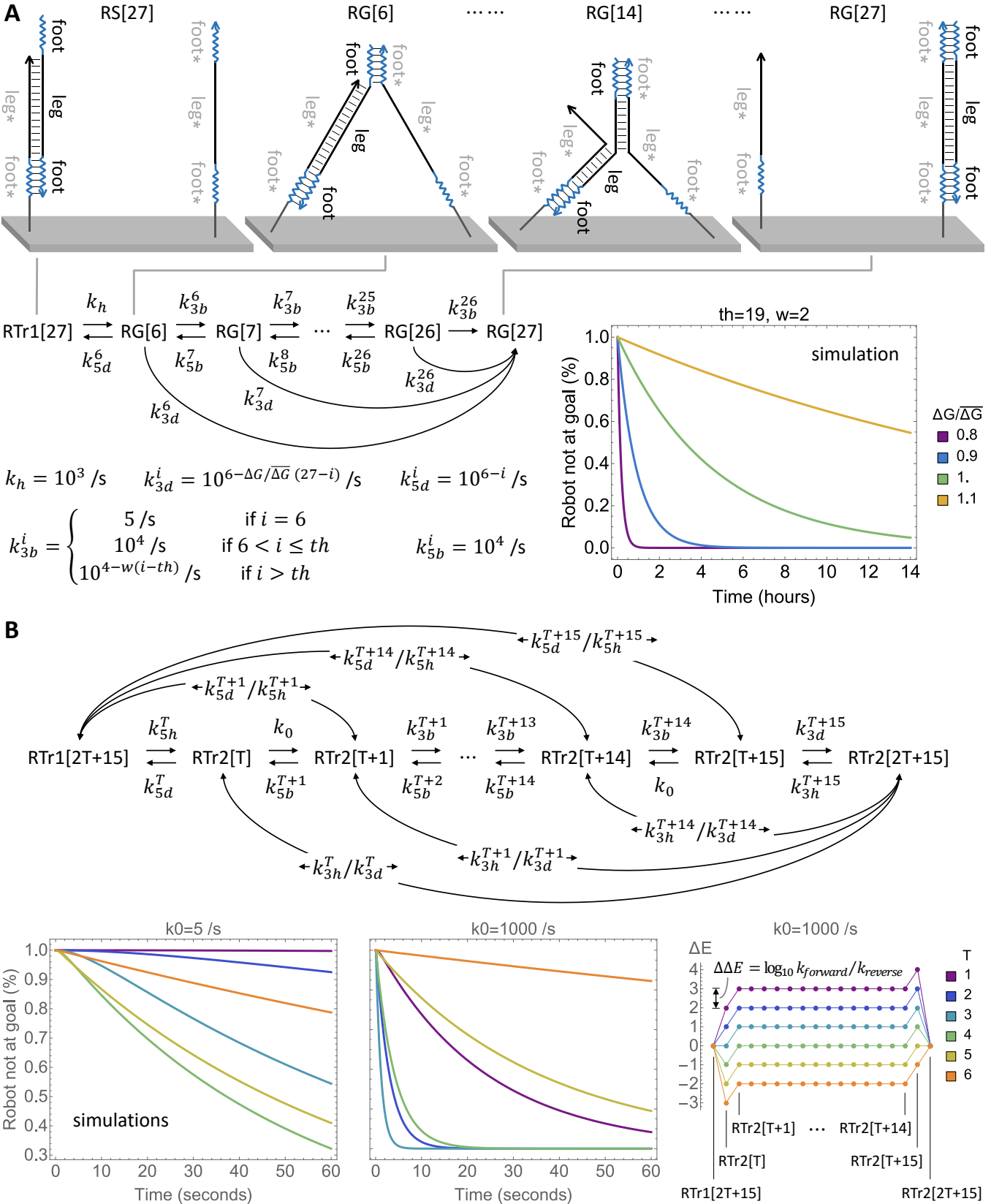


Fig. S3. A biophysical model of the walking mechanism. (A) Model and simulation of an irreversible pathway for the robot taking one step to reach the goal location. **(B)** Model of an reversible pathway for the robot taking one step from a track location to another, and simulations of two steps of walking to a goal, with $th = 19$, $w = 2$, and toehold lengths (T) from 1 to 6.

2.4 The purity of DNA origami affects the completion level of desired reactions

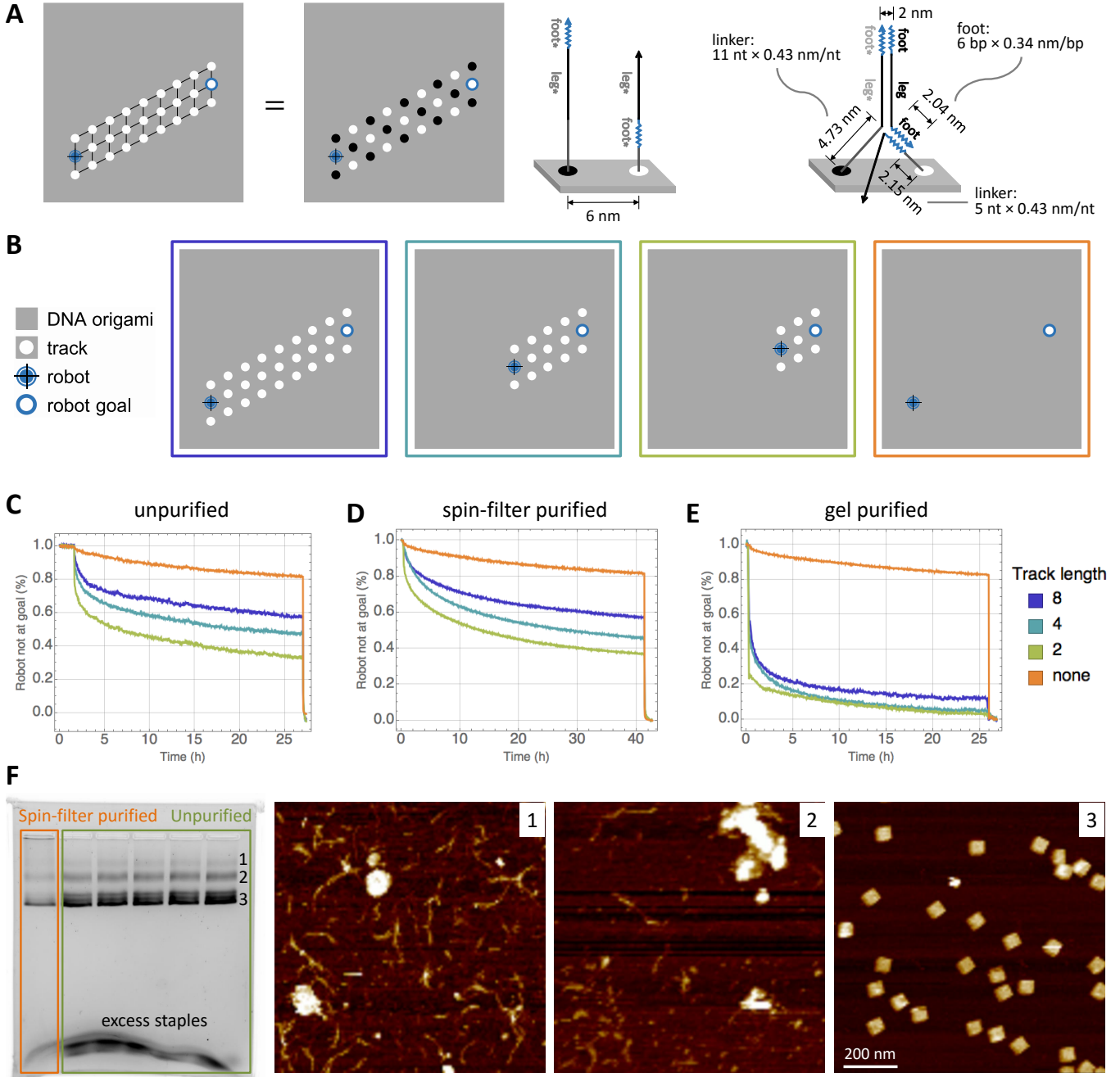


Fig. S4. The purity of DNA origami affects the completion level of desired reactions. (A) The checkerboard layout of two distinct types of track strands in all random-walking systems. The lengths (11 and 5 nt) of the linkers in the two types of track strands are designed to allow the robot to reach an adjacent track location: $4.73 + 2 + 2.04 + 2.15 = 10.92 \text{ nm} > 6 \text{ nm}$. (B) Schematic diagrams of the robot walking on linear tracks of three distinct lengths and a negative control with no track. Fluorescence kinetics data of the setup shown in A, using (C) unpurified, (D) spin-filter purified, and (E) gel purified double-layer DNA origami. (F) Spin-filter purified and unpurified origami on an agarose gel and AFM images of the three labeled bands extracted from the unpurified lanes on the gel. Band 3 was subsequently used for all gel-purified samples. To obtain enough DNA structures after gel purification, we used five lanes of the same unpurified sample. We assumed that the three bands in the spin-filtered lane had the same types of DNA structures shown in the AFM images, because the locations of the bands were identical compared to the unpurified lanes. The scale bar applies to all three images.

2.5 Numerical analysis of the random walk

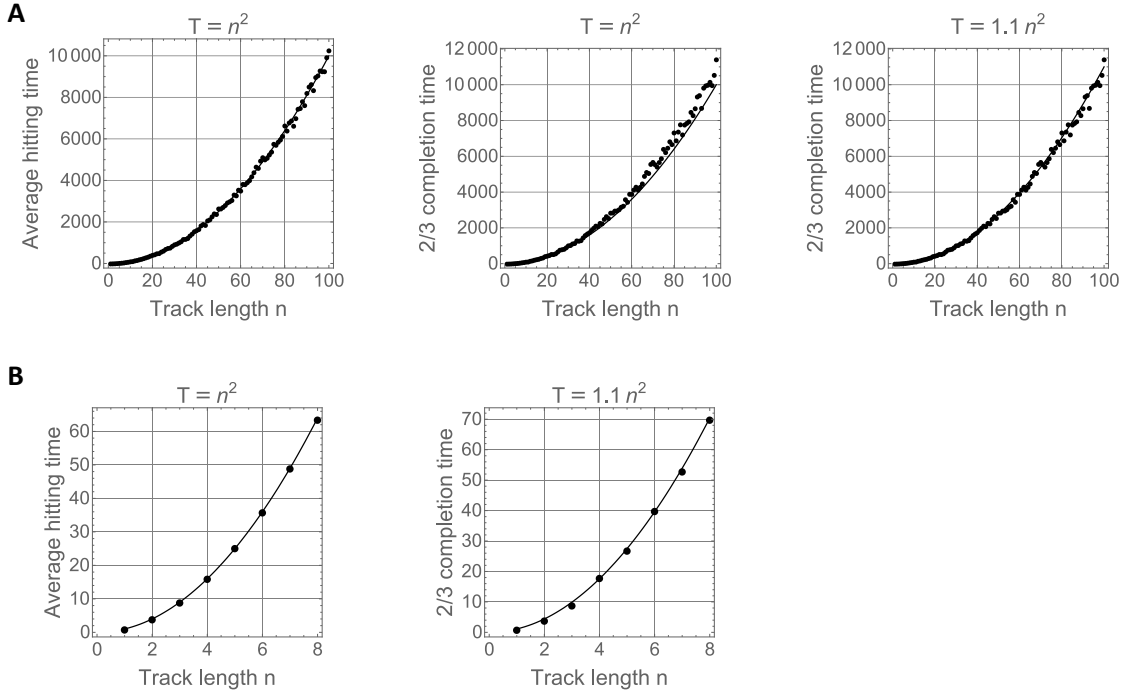


Fig. S5. Numerical analysis of the random walk. Average hitting time and two-thirds completion time of random walks on linear tracks of lengths 1 to n , with (A) $n = 100$ and 1,000 trials for each track length, and (B) $n = 8$ and 10,000 trials for each track length. The linear track consists of sites $0, 1, 2, \dots, n$. The random walk starts at site 0. For any site $0 < i < n$, the random walk moves to $i - 1$ or $i + 1$ with equal probability. If the random walk returns to 0, it continues to 1. The hitting time is defined as the number of steps for the random walk to hit site n for the first time. The average hitting time is the mean of the hitting time for all trials. The two-thirds completion time is the smallest number of steps that is greater than or equal to the hitting time for two-thirds of all trials.

The average hitting time (also referred to as the first-passage time) of a random walk on a linear track has been well studied (31, 57). However, the average hitting time cannot be directly read off from experimental data, unlike the related notions of the fractional completion times, such as the half-completion time (i.e. the median hitting time) and the two-thirds completion time. For random walks in general, these quantities can behave quite differently and we are not aware of direct mathematical relationships that allow calculating one from the other. Therefore, we performed numerical simulations of one-dimensional random walks to establish that, in the case relevant to our experimental investigations, the two-thirds completion time scales quadratically with the track length, just like the average hitting time.

For track lengths $n = 1$ to 100, numerical simulations of 1,000 trials per track length confirmed that the average hitting time T is quadratically related to n (Fig. S5A, left). The two-thirds completion time is fairly similar to the average hitting time (Fig. S5A, middle), but can be better estimated as $T = 1.1n^2$ (Fig. S5A, right). Taking a closer look at track lengths $n = 1$ to 8 (which are the lengths used in our random walk experiments) with numerical simulations of 10,000 trials per track length, $T = n^2$ is practically an exact function for the average hitting time while $T = 1.1n^2$ remains a very good estimate for the two-thirds completion time (Fig. S5B). Thus, we concluded that it is reasonable to apply a quadratic fit to the two-thirds completion time extracted from the experimental data, and use that to determine the rate constants in the mass action simulation of the reactions involved in our random walk system.

2.6 Cargo pick-up

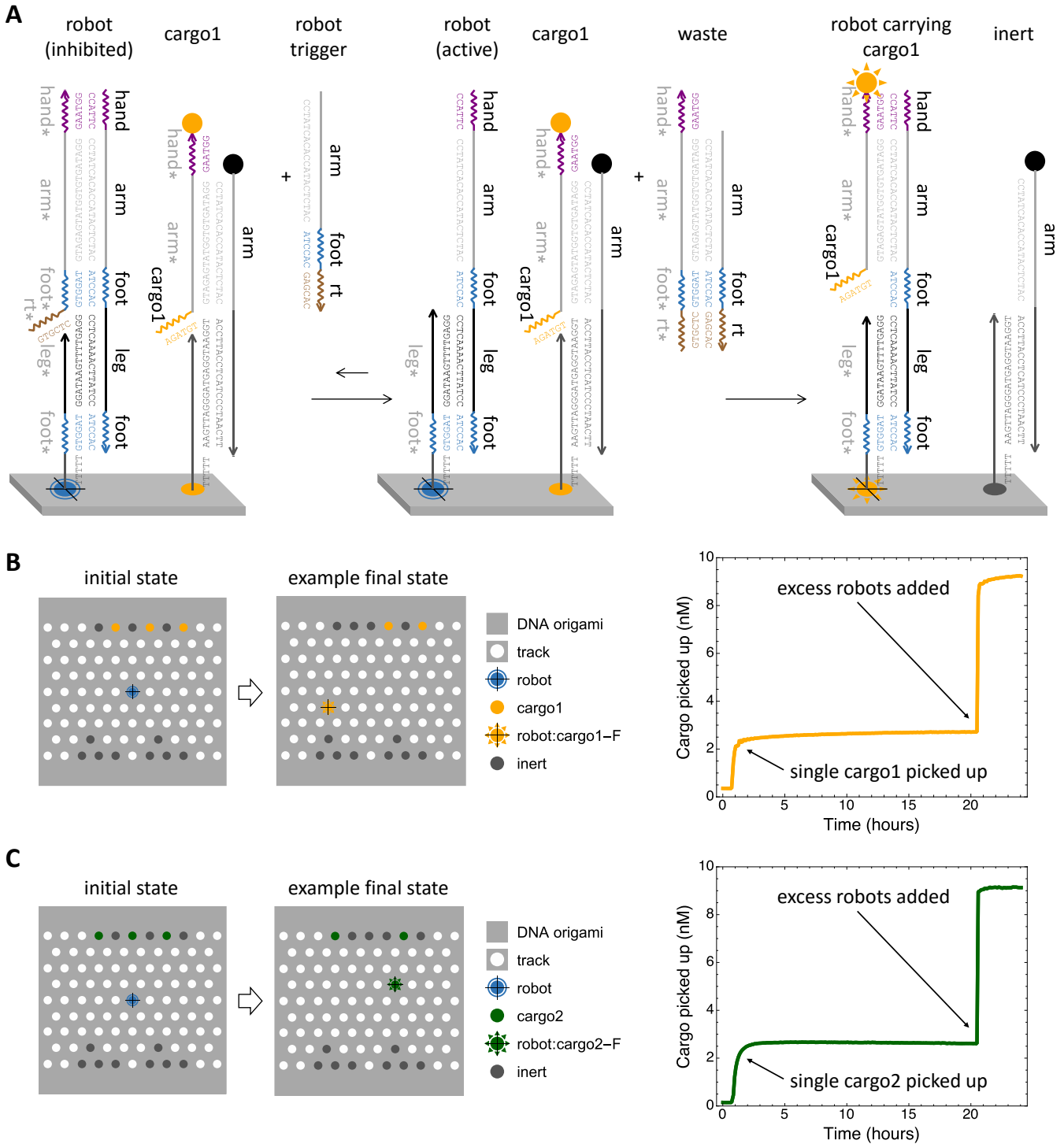


Fig. S6. Cargo pick-up. (A) Sequence-level diagram of the mechanism of the robot picking up a cargo after being triggered. The processes of cargo pick-up are identical for both types of cargos, and the only difference is the sequence of the cargo domain on the cargo strand. Two distinct sequences, AGATGT and GAAAGG, are assigned to cargo1 and cargo2 domains, respectively. Schematic diagram and fluorescence kinetics data of the robot picking up (B) cargo1 and (C) cargo2. The cargo strands are labeled with a fluorophore and cargo attacher strands are labeled with a quencher. When a cargo is picked up from its initial location, the fluorescence signal increases.

2.7 Procedure for preparing cargo-sorting samples

Step 1: anneal origami with excess staples and cargo strands.

Step 2: gel purify origami and remove excess staples and cargo strands.

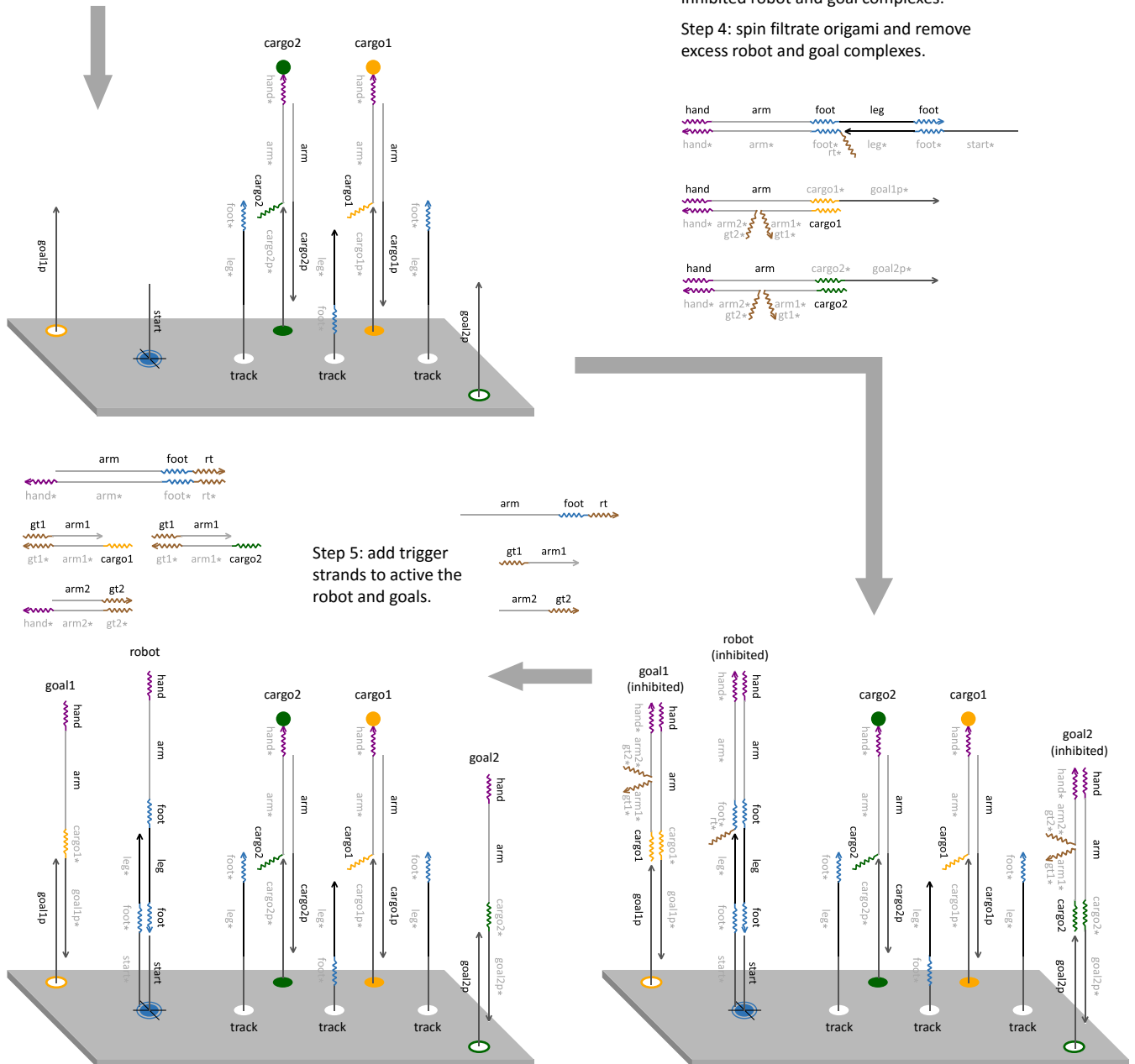


Fig. S7. Procedure for preparing cargo-sorting samples. Step 1: anneal origami with a 10-fold excess of the regular, track, robot start, cargo and goal staples, 11-fold excess of the cargo attacher strands, and 12-fold excess of the cargo strands. Step 2: gel purify origami to remove malformed structures, and excess staples and cargo strands. Step 3: incubate origami with an approximately 2-fold excess of gel-purified inhibited robot and goal complexes, assuming a 50% yield from gel purification. Step 4: spin filtrate origami to remove excess robot and goal complexes. Step 5: add a 20-fold excess of trigger strands to active the robot and goals. For more details see materials and methods.

2.8 Negative control for cargo sorting without a robot

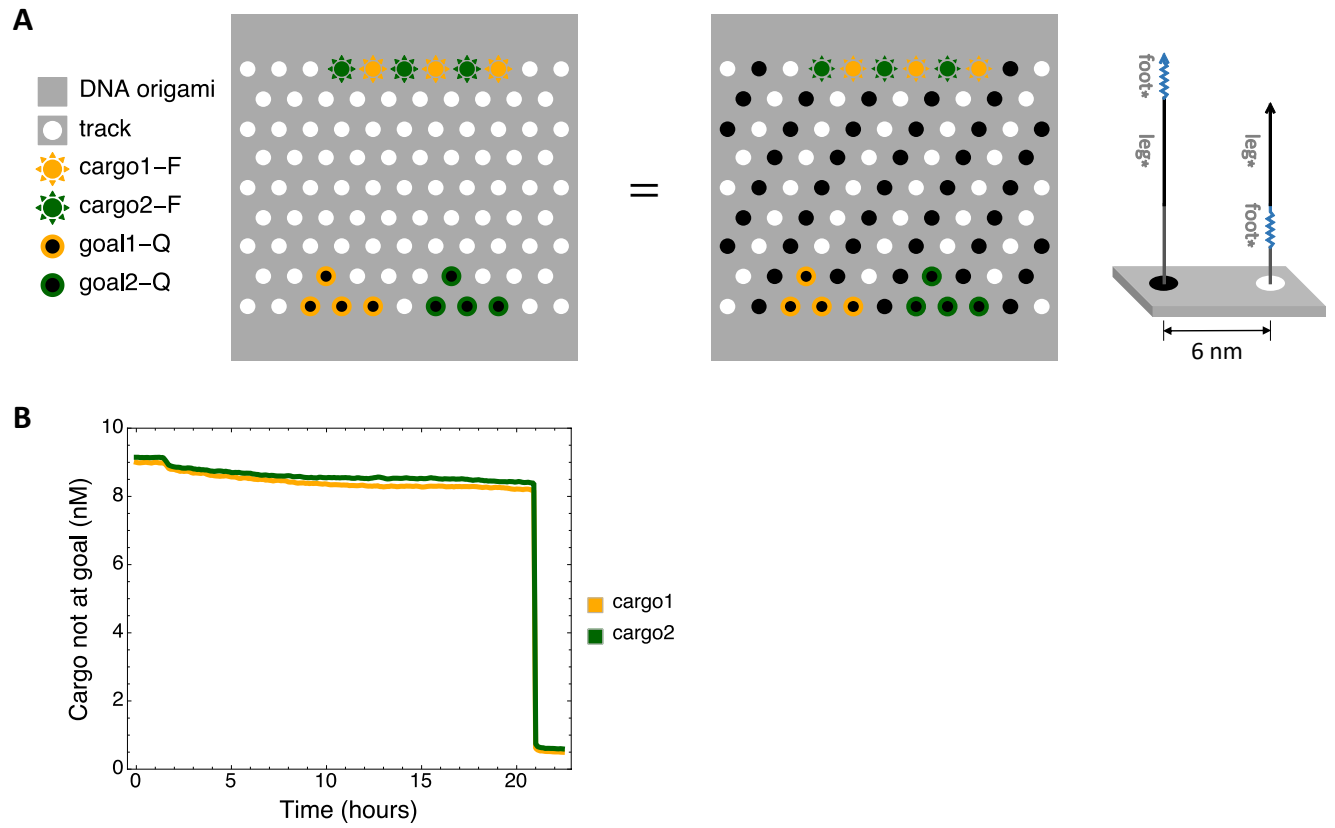
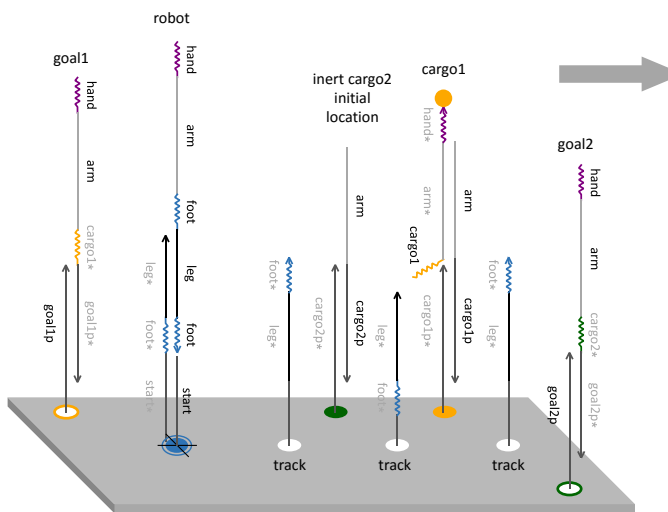


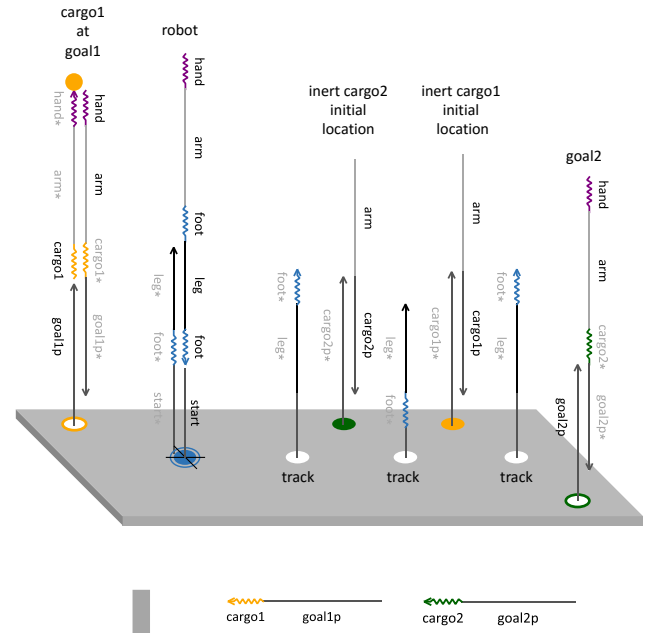
Fig. S8. Negative control for cargo sorting without a robot. (A) Schematic diagram of the negative control experiment, and the checkerboard layout of two distinct types of track strands in all cargo-sorting systems. (B) Fluorescence kinetics data of the negative control experiment. The two types of cargos are labeled with two distinct fluorophores, and the two types of goals are both labeled with a quencher. When a cargo is dropped off at a goal location, the fluorescence signal decreases.

2.9 Procedure for preparing cargo-sorting samples for AFM imaging

Initial state of the cargo-sorting experiment
with one type of cargo and two types of goals.



Final state of the cargo-sorting experiment
with one type of cargo and two types of goals.



Step 1: add remover strands for both types of goals, and goals without a cargo will be removed.

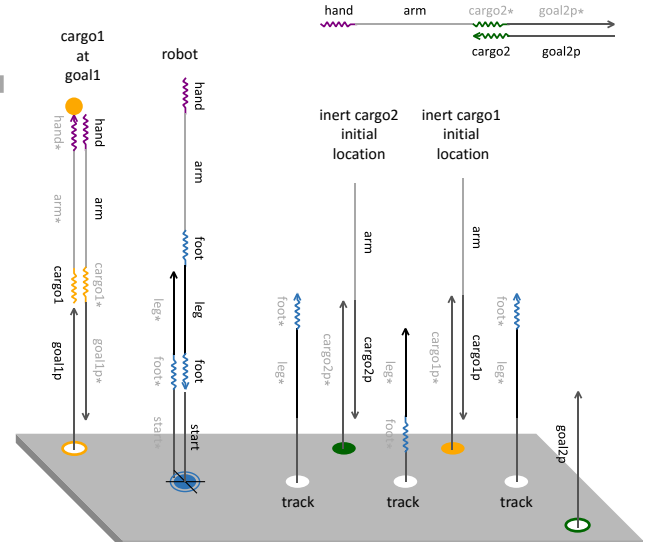
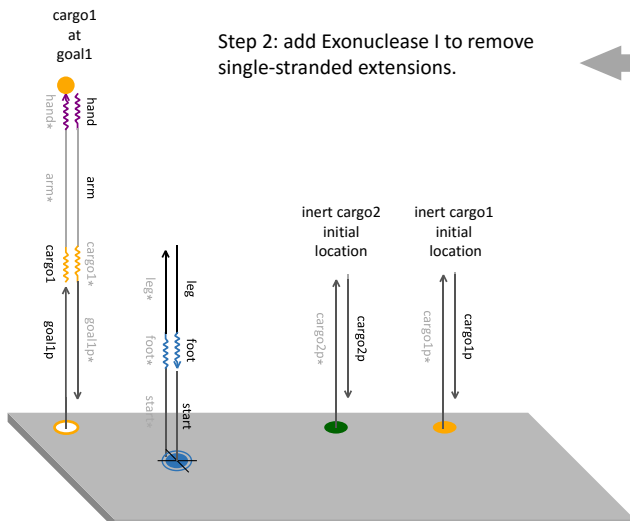
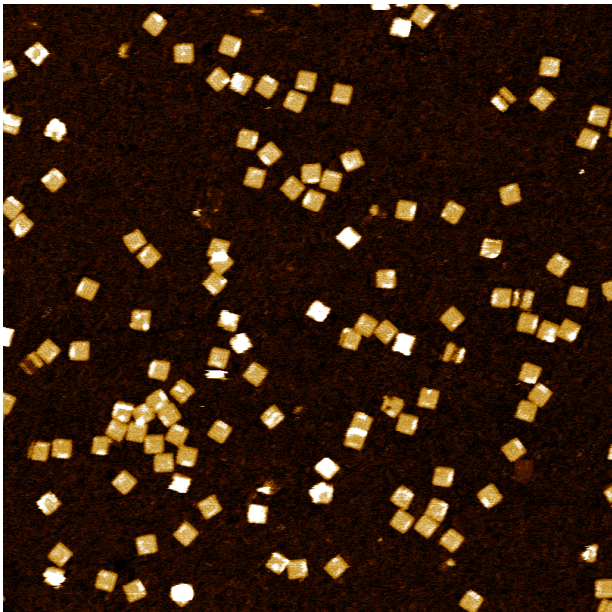


Fig. S9. Procedure for preparing cargo-sorting samples for AFM imaging. The initial locations of both cargo types are used as a reference for recognizing the orientation of origami in AFM images. Step 1: add a 20-fold excess of remover strands for both types of goals to remove goals without a cargo. Step 2: add Exonuclease I to remove single-stranded extensions and create a clean background for imaging the locations of the cargos at goals. For more details see materials and methods.

2.10 AFM images of the cargos at their initial locations and destinations

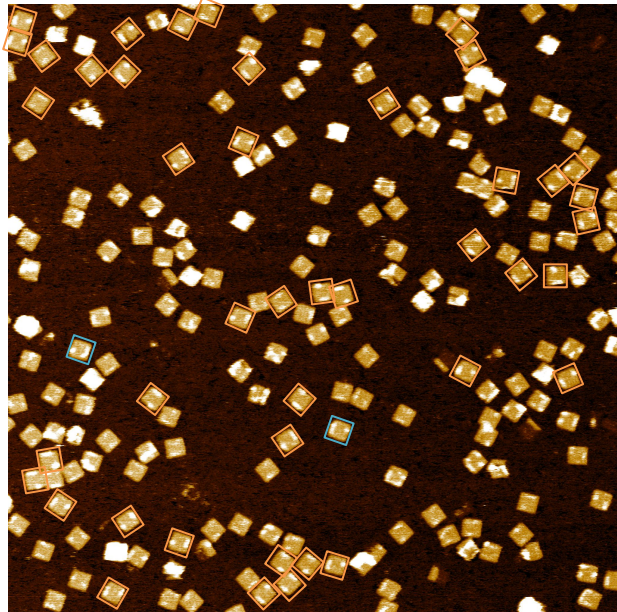
A

cargo1 at initial location (before sorting)



B

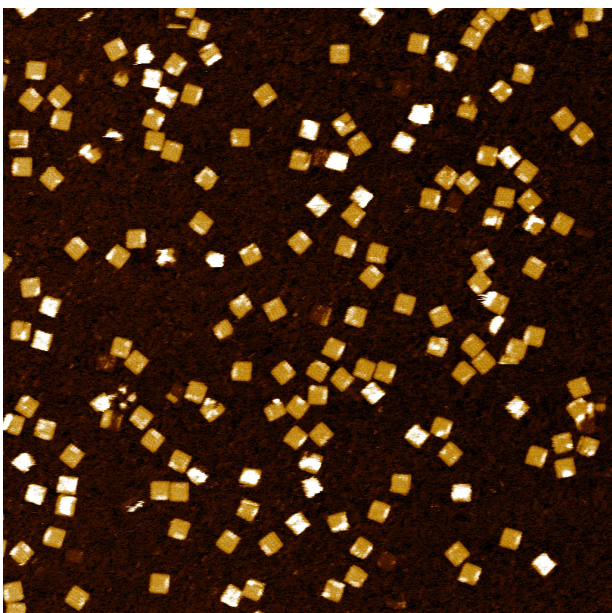
cargo1 at destination (after sorting)



over or under digested: 194 (81%)
correct: 43 (18%) ambiguous: 2 (1%) incorrect: 0 (0%)

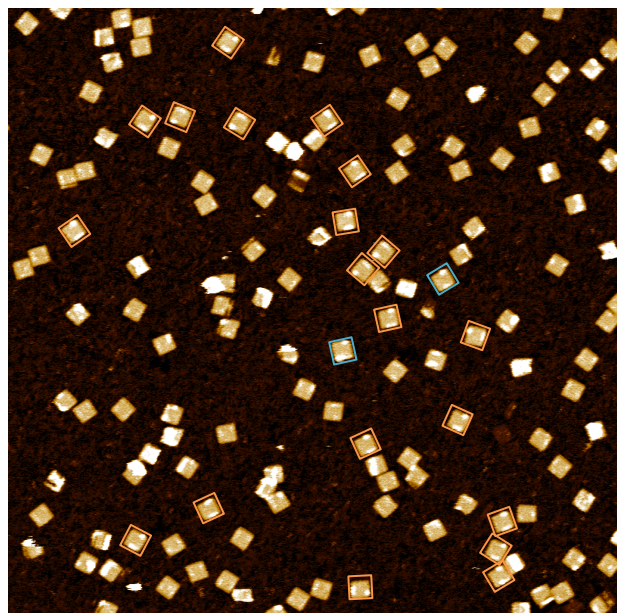
C

cargo2 at initial location (before sorting)



D

cargo2 at destination (after sorting)

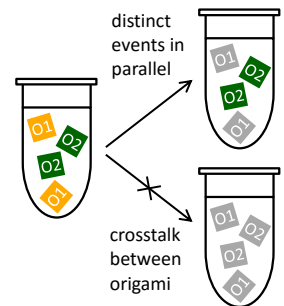
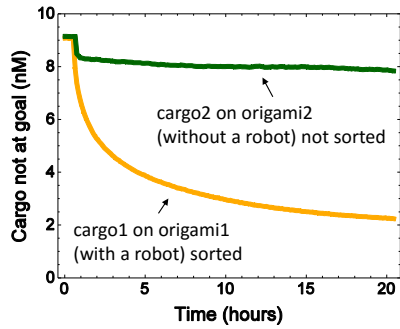
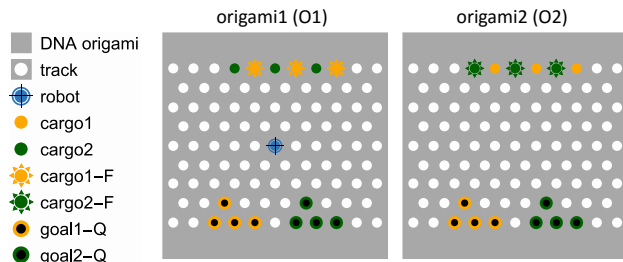


over or under digested: 137 (86%)
correct: 20 (13%) ambiguous: 2 (1%) incorrect: 0 (0%)

Fig. S10. AFM images of the cargos at their initial locations and destinations. (A) Cargo1 at initial location. (B) Cargo1 at destination. (C) Cargo2 at initial location. (D) Cargo2 at destination. All AFM images are 2 by 2 μm in size. If an origami does not have clearly recognizable molecules both at the initial location and at either of the two destinations, it is classified as *over or under digested* by Exonuclease I. Otherwise there are three situations: If the destination looks like the correct one (i.e. goal1 for cargo1 or goal2 for cargo2), it is classified as *correct*. If it is hard to tell whether the destination looks correct (for example, because the lack of clear asymmetry of the molecules at the initial location), it is classified as *ambiguous*. If the destination looks like the incorrect one (i.e. goal2 for cargo1 or goal1 for cargo2), it is classified as *incorrect*.

2.11 Cargo sorting with mixed populations of DNA origami

A



B

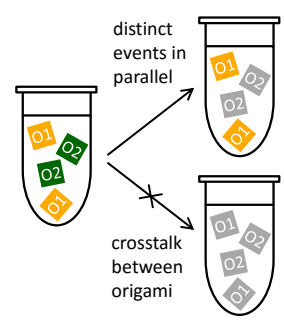
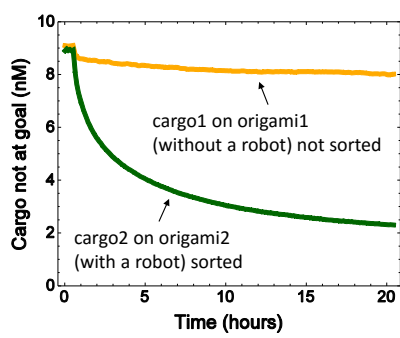
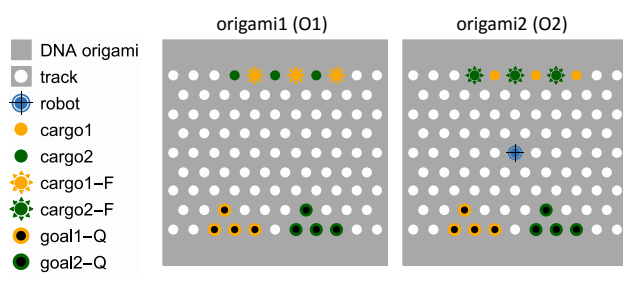


Fig. S11. Cargo sorting with two mixed populations of DNA origami, one with a robot and the other without. Schematic diagram and fluorescence kinetics data of (A) origami1 with a robot and origami2 without, and (B) origami2 with a robot and origami1 without. Origami1 has cargo1 labeled with a fluorophore and cargo2 left unmodified. Origami2 has cargo2 labeled with a fluorophore and cargo1 left unmodified. If the robot stays on the origami on which it is initially placed, the sorting of one type of cargos will be detected but not the other.

2.12 Analysis of the completion levels in the cargo-sorting experiments

The explanations for the linear model, from top to bottom in Supplementary Fig. S12A, are the following:

In the experiment shown in Supplementary Fig. S8, because there is no robot, the only possible reaction that yields a decreased fluorescence signal should be a goal on one origami picking up a cargo on another.

In the pair of experiments shown in Fig. 3B, the completion levels of the desired cargo-sorting reactions tell us the maximum fraction of cargos that can be correctly sorted and the baseline of zero.

In the pair of experiments shown in Fig. S11, there are two populations of origami: one has a robot (origami1) and another does not (origami2). Only one type of cargo is labeled with a fluorophore on each type of origami, but both types of goals have a quencher. If a robot moves from origami1 to origami2, the monitored type of desired cargo sorting on origami1 will decrease because the same type of cargo on origami2 does not have a fluorophore. A robot or goal on origami1 picking up a cargo on origami2 should not affect the completion level — since we have four goals and three cargos per type per origami, an additional cargo would just occupy the extra goal location. A goal on origami2 picking up a cargo on origami1 should not affect the completion level either, because the goal on origami2 also has a quencher and it is no different from the goal on origami1. Simultaneously, the monitored type of undesired cargo sorting on origami2 will increase if a robot moves from origami1 to origami2 and start sorting the cargos, or if a robot or goal on origami1 picks up a fluorophore-labeled cargo on origami2.

In the experiment shown in Fig. 4A, there are also two populations of origami: only one type of cargo is labeled with a fluorophore on each type of origami, and only the corresponding type of goal has a quencher. If a robot or goal on one type of origami picks up a fluorophore-labeled cargo on the other type of origami, there will be no signal change since the corresponding goal has no quencher. Because both types of origami already have a robot, an additional robot moved from another origami should not affect the completion level of the desired cargo sorting. Loosing a robot to another origami should occur much slower than the desired local cargo sorting reactions, and will not affect the completion level if the event takes place after the cargos are already sorted on the original origami.

	Completion level of cargo1 (%)	Completion level of cargo2 (%)	Linear model
Fig. S8	8.65	7.85	z
Fig. 3B	79.02	81.15	max
	2.72	0.88	0
Fig. S11	75.16	74.07	$max - x$
	12.11	14.09	$x + y + z$
Fig. 4A	62.29	64.49	$max - y - z$

		Completion level (%)
Robot moving from one origami to another	x	1.59
Robot on one origami picking up cargo on another	y	4.56
Goal on one origami picking up cargo on another	z	8.25

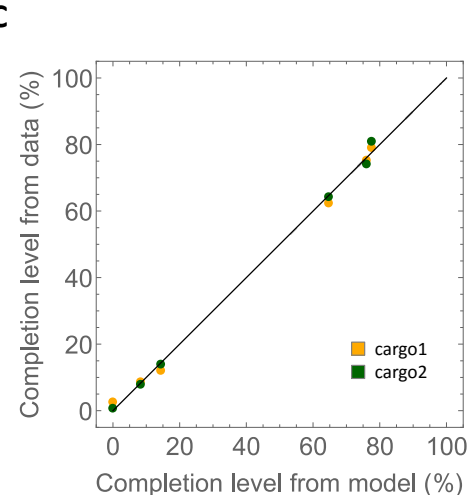
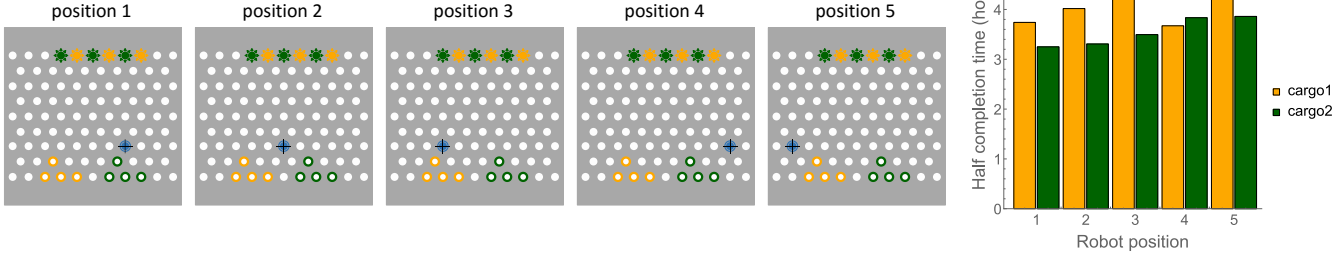


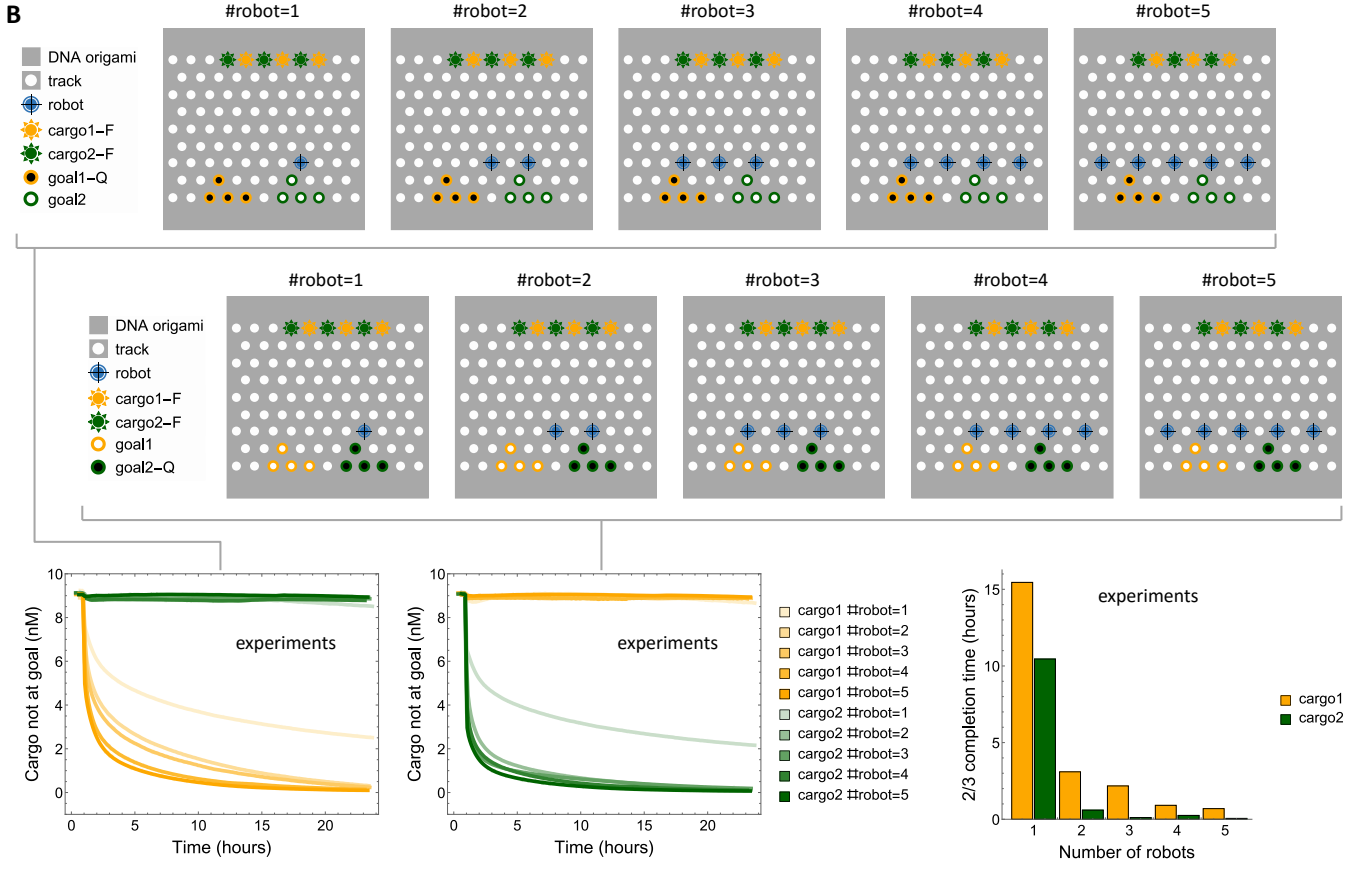
Fig. S12. Analysis of the completion levels in the cargo-sorting experiments. (A) Completion levels at the 20-hour time point from the experimental data, and our interpretation of the completion levels in a linear model for analyzing undesired inter-origami interactions. (B) The definition of the variables in the model, and the values from a linear least-squares fit using the four variables and twelve data points. max was fitted to be 77.5%. (C) Comparison between the model and the data.

2.13 Multiple robots collectively performing a cargo-sorting task

A



B



C

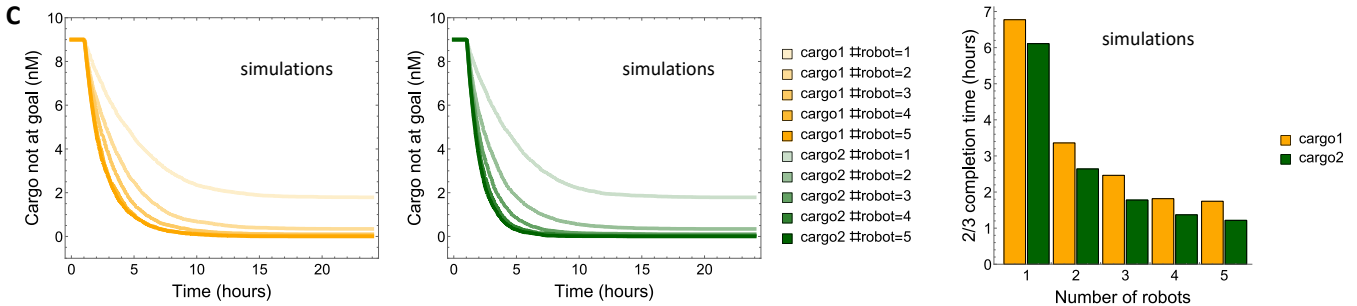


Fig. S13. Multiple robots collectively performing a cargo-sorting task. (A) Simulations of cargo sorting with a single robot at five distinct initial locations. The robots are ranked based on how long it takes for them to sort the cargos, from the fastest to the slowest. (B) Design diagrams and fluorescence kinetics data of cargo sorting with one to five robots. (C) Simulations with each robot being present with a 80% probability. In each case, the additional robot is predicted to be slower than the existing robot(s), so we know that the increased overall speed for cargo sorting is caused by the collective behavior of the robots.

3 Cadnano diagram

3.1 Double-layer square DNA origami design

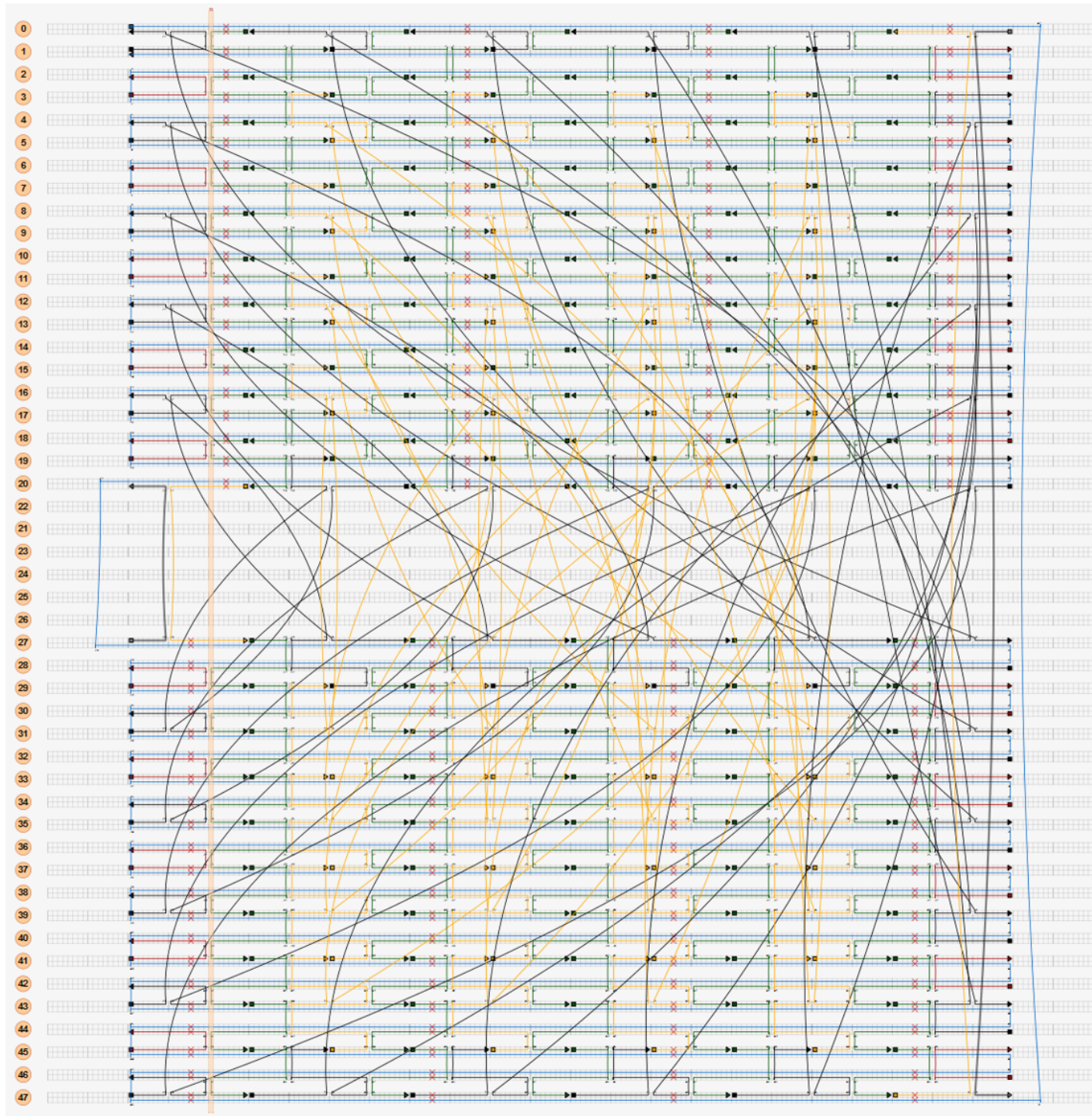


Fig. S14. Double-layer square DNA origami design.

4 DNA sequences

4.1 Staples

Table S1: Staples in the double-layer square DNA origami.

Name	Sequence
T C01 R01	GGCGATGGCCCCTAGAAAAACCAACGGGGT
T C01 R02	AACGGTACGCCAGAATAGGGATTTAGACAGG
T C01 R03	AAGAATACTGTCACATCTGACCTATGATAACAGGAGTGT
T C01 R04	TTGAGGATTAGAAGTTCAATAGATAATACAT
T C01 R05	ATAACGGATTGCCCTGTACATGCCGTTCCAGTAAGCG
T C01 R06	TAGGTTGGTTATATATTTAACCTCCGGCT
T C01 R07	GTACCGACAAAAGGTAATAAGAGAGCCAGAATGGAAAGC
T C01 R08	CGGGAGGTTTGAAGCCGAACCTCCGACTTG
T C01 R09	AACAATGAAATAGCAAATAATAATGATATTACAAACAA
T C01 R10	GGTGAATTATCACCGTGAATTATTACATTAAA
T C02 R01	AAAGGGCGTGAACCATCACCCAGGAGGC
T C02 R02	CGATTAACCTGAGAAGTGTTCAGAGATA
T C02 R03	GAACCTGACAATATTTGAAAATAGATT
T C02 R04	AGAGCGATTAGACTTACAAAAGTAACAG
T C02 R05	TACCTTATTGCTTGAATACCGTCTGAGA
T C02 R06	GACTACCACTATATGTAATGCCATTTCG
T C02 R07	AGCCAGTAAGTAATTCTGTCCACGCGAGGC
T C02 R08	GTTTAGCTTAAATCAAGATTAAATTGAGT
T C02 R09	TAAGCCCTAGCTATCTTACCGAAGGTAAT
T C02 R10	ATTGACGCACCGACTTGAGCCACACCTCA
T C02 R11	GAGCCGCCACCAGAAAGGAGGTTGAGGCAG
T C03 R01	TTTTTGGTTAAAGAATTGGTCG
T C03 R02	GTGAGGCCAGAGCGGGAGCTAAAAATCAAG
T C03 R03	AGTCTTTAGGGACATTCAACAACCCCTCATAGTTAGCGTACAATAGGA
T C03 R04	CAACTCGTAGGAGCACTAACAACTGGCTATT
T C03 R05	AAATCGCGCTCAGATAGCTTGATCGTCTTCAGACGCCACCACC
T C03 R06	ATCCAATCTTATCAAATCATAGAAGTTACA
T C03 R07	CAATAAACGTAAATTAAATCAGCTTCTGTATGGGATTTGCAACCGCCA
T C03 R08	TTTGCACCTCCGGTATTCTAAGAAGACGACGA
T C03 R09	TTAAGAAAAGAGATAACTCCAAAAGTTTCAGCGGAGTGATACTCAGG
T C03 R10	TTAGAGCCCCGATTGAGGGAGGGAAAGCCCTT
T C04 R01	GTCCACTAGGTCGAGGTGCCGTAACTTTCTC
T C04 R02	GTTAGAATACCGAGTAAAAGAGTCACGACCAAG
T C04 R03	TAATAAAAATGCGCGAACTGATAGTATCTAA
T C04 R04	ATATCTTATTAAATCCTTGCCAGATTTC
T C04 R05	AGGTTAACAGAGGCATTATTCAAGAGTCA
T C04 R06	ATAGTGAAGCAAGACAAGAACGCTTAACAAAC
T C04 R07	GCCAACATAACATGTTAGCTAATAGATATAG
T C04 R08	AAGGCTTACAGCTACAATTATCTGAGCGCT
T C04 R09	AATATCAGAGTAAGCAGATAGCCAAAGGGCG
T C04 R10	ACATTCAAAGCAAATCACCAGTAGCCACCC
T C04 R11	CAGAACGCCACCCCTTTTCACTAAAGGAATTGCGA
T C05 R01	AATCGGAATGTTGTTCAATTACAGG
T C05 R02	CACGCAAAGCACGTATAACGTGAGCACTA
T C05 R03	ACATGCCAGATTCCACCGTTAATAGAAAGAGGACAGATGATCCGCGAC
T C05 R04	ATTAATTGGAATTGAGGAAGGTCCCTAAA
T C05 R05	TTACCTGAATAAAGAATACCAAGTGCATAGGCTGGTTGTATCA

Name	Sequence
T C05 R06	CTTTTCAGATTAAGACGCTGAGATTCAA
T C05 R07	GCGCCTGTTGAGAATCTACCTTATAATCTTGACAAGAACCATACCAAG
T C05 R08	TTACCAACAATAGCAAGCAAATCGCAGAAC
T C05 R09	TTACCCAGAAAGTCAGATGGTTAAAAATCAACGTAACAAACTAAAACA
T C05 R10	TACCATTACCAGCGCCAAGACAAACAAAG
T C06 R01	GGGTTGAGCCCTAAAGGGAGCCCTATGGTTG
T C06 R02	CTTGACGTTAACCGTTGTAGCAAGATTATT
T C06 R03	ACATTGGCATTAAAAATACCGAACAAATCAAC
T C06 R04	AGTTGAAATAAAAGTTGAGTAACCGCACGTA
T C06 R05	AAACAGAACGAAAAGAAGATGATGACATAGCG
T C06 R06	ATAGCTAAATATATTAGTTAAAACAGTAG
T C06 R07	GGCTTAATTATCAACAAATAGATAAATCATTA
T C06 R08	CCCGGCCGCTAACGAGCGTCTTCTGAACAC
T C06 R09	CCTGAACAAGGAAACCGAGGAAACAAATTCA
T C06 R10	ATGGTTTAGCAAGGCCGAAACGTAGCCACCA
T C06 R11	CCGGAACCGCCTCCCTCACCGAGATAAGGCTGCCCTG
T C07 R01	AGCTTGACAAATCAAATTGGGGC
T C07 R02	TGATTAGTGCTACAGGGCGTACCGATTAG
T C07 R03	AGCAGAAGTCATCGTATGGTCATCAAATATCGCGTTTCAGGTCT
T C07 R04	TTTGC GGATATCTGGTCAGTTGGGAACCACC
T C07 R05	ATCAAGAACCATATCAATTAGTCGAACCAGACCGGAATCAGAAAA
T C07 R06	TCTGACCTCTAGAATCCTGGAAAAAACAAAC
T C07 R07	ACAAGAAATATAAAGCAACAGTTGCAGGATTAGAGAGTACTCATTGAA
T C07 R08	TAATTTGCTTATTTCATCGTAGGAGTCCTGA
T C07 R09	AACCGAATTAGACGGGAAGTACGGTTGATAAGAGGTATTGCTCAA
T C07 R10	AAACCATCTGTCAAAATCAATAGAGCAATAAT
T C08 R01	CCCTTATGGGGAAAGCCGGCAGCGCTTA
T C08 R02	ATGCGCCAATAACATCACTTGCCTACATT
T C08 R03	TTGACGCATAAAACAGAGGTGACAAACCCCT
T C08 R04	CAATCAAACAAAGAACCAACCAAGGGTTA
T C08 R05	GAACCTAAACAAAATTAAATTACATTAATTAA
T C08 R06	ATTTCCAATTAAATTGTTGACAAATT
T C08 R07	TTACCCAGATAATATCCATCCACAAGCAA
T C08 R08	GCCGTTTCAGTTACAAAATAAAACAGGGAA
T C08 R09	AGCGCATACCCAAAAGAACTGGGGATAAG
T C08 R10	TTTATTGATAGCAGCACCGTAATCTTTC
T C08 R11	ATAATCAAATCACCTGTAGCTAGCTTAATTGCTGAA
T C09 R01	AGAAAGGATGGTGGTTAACAAACG
T C09 R02	AAGAACTCTAACCAACACCCGCACGTGGCG
T C09 R03	GTATTAACACGCTCAGCGAGTAAGTCATTGCCCTGAGAGTATGATATT
T C09 R04	GGAATTATGCTGAACCTCAAATATGGCGGTCA
T C09 R05	ATTTCATTACTTCTGTGTAGCCAAATCGATGAAACGGTAAAGGCCG
T C09 R06	ACCGTGTGTCTGTAATCGTCGCTATTAAACA
T C09 R07	GAGCATGTGTATCATA CGCCATCAGTCATATGTACCGTAATGTG
T C09 R08	TTATTTATACCGCACTCATCGAGATAATTAC
T C09 R09	AGACTCCTGAGAGAAATTAAATCAAAAGCCCCAAAACAAACCCCTCA
T C09 R10	CGACAGAAAACGCAAAGACACCACCATGATTA
T C10 R01	CTGTTGAAGGGAAAGAAAGCGAAAGCGGTAC
T C10 R02	GCTGCGGAAACTATCGGCCTTGCCCATTGCA
T C10 R03	ACAGGAAAACGCCCTGCAACAGTGTCTAAAGC
T C10 R04	ATCACCTTCATCATATTCTGATTCTGATTGT
T C10 R05	TTGGATTATGAATTACCTTTTAAGTGAATA
T C10 R06	ACCTTGCTATAATAAGCGTTAAAGAAAAAG

Name	Sequence
T C10 R07	CCTGTTAAGAAACCAATCAATAAGGGTATTA
T C10 R08	AACCAAGTCCAATCAAATAAGAAATAGCAG
T C10 R09	CCTTACATATTACGCAGTATGTTGGCAACAT
T C10 R10	ATAAAAGATCAAGTTGCCTTAGTTCGGT
T C10 R11	ATAGCCCCCTATTAGATATTTAAATATTAAATTGT
T C11 R01	GTTGCCCGCAGCAAG
T C11 R02	GCGCTGGCAAGTGTAGGAGCGGGCGCTAGG
T C11 R03	CAATATTATTGCCCTTCGTAATCATGGTCATGTTGTAAA
T C11 R04	GCAGCAAATGAAAAACCACGCTGAGAGCCA
T C11 R05	TTCATCAATCTTCAAATTGTTATCCGCTGGGTAAAC
T C11 R06	AAATCAATATAATGTGATGAAACAGTACAT
T C11 R07	GGAATCATGCGGTTGATACGAGCCGAAGCACGAAAGGG
T C11 R08	TATCATTCCAAGAACTCGGCTGTCTTCCT
T C11 R09	AACGTCAACATTAATGGGGTGCTAATGAGTGTGCGGGC
T C11 R10	TACATACATAAAGGTAGCAAACGTAGAAAA
T C11 R11	CGTTTCATTCCAGATTGCGTTGCGCTCA
B C01 R01	GCATTGACCCACCACC
B C01 R02	ATAAGTATAGCCC GGTCGAGAGGGTTGAT
B C01 R03	ATAATAATAGAGCCACTTGGGAA
B C01 R04	CAACCTAAAACGAAACCAC TACGAAGGCAC
B C01 R05	ACGAGAAACAGAGCGCACCAT
B C01 R06	GGGGGTAATAGTAAAAGAAGTTTGCCAGA
B C01 R07	TATAATGCGGAACCAGCACCAATG
B C01 R08	TTTATTTCACGCAATTGCGGGAGAACGCC
B C01 R09	AAACGTTACGTTGCCATCAGTAG
B C01 R10	CAGGCTCGCAACTGGCGCCATTGCCATT
B C01 R11	CTGCCCCTCGGCATCGTCAGACTGTAGCG
B C02 R01	GTCAGACGCAGGCGGATAAGTGCACATAGGT
B C02 R02	TATCACCGGAATAGAAAGGAACACGTTGAAA
B C02 R03	ATCTCCAAGGTAAAATACGTAATGGAGGCAAA
B C02 R04	AGAATACAGCTGCTATTCACTGAAACGAGTAG
B C02 R05	TAAATTGGGAGAGGCTTTGCAAATGTTAG
B C02 R06	ACTGGATATTGCGGATGGCTTAGCAACATGT
B C02 R07	TTAAATAATGACCCCTGTAATACTGGATAAAA
B C02 R08	ATTTTAGGGAAGATTGTATAAGCGTTAAAAT
B C02 R09	TCGCATTACCGGAAACCAGGCAAATTGGGAAAG
B C02 R10	GGCGATCGGAGCTAACTCACATTATCGGGAAA
B C02 R11	CCTGTCGTGCCAGCTGAAATGAAAACGATTTTGT
B C03 R01	AGGTTAGGGTTTGTCAAGTACATTGGCTGAGCAAGA
B C03 R02	CTCATCTTAAGTTCCATTAAACGAAAAAAGGCCACAAGGTTGCTAT
B C03 R03	TACTCGGTAACCAAAATAGCGCTGAGAGGTAATCTGAATC
B C03 R04	TATATTTTGTACCAAAACATTGCAACTAAGAATTAACCAGAGCC
B C03 R05	CTCTCGCGGCCACCGCTCTGGTAATTGAAACATAAACAGCCATA
B C04 R01	ATAAAATCGGATTAGGATTAGCGTACCGCCA
B C04 R02	CCCTCAGTAAACAACCTTCAACGGAGCCTT
B C04 R03	TAATTGTGACTTTTCACTGAGGTGACCCCC
B C04 R04	AGCGATTGGATATTCAATTACCCCTTCAACT
B C04 R05	TTAATCATTACCAAGACGACGAAATCGTCA
B C04 R06	TAAATATCTTAATTGCTCCTTGTCTGGA
B C04 R07	AGTTCAATAAGCTAAATCGGAATGCAA
B C04 R08	TGCCTGACCGGGITGATAATCAGGCTCATT
B C04 R09	TTAACCTCCAGCCAGCTTCCTATTACGC
B C04 R10	CAGCTGGTAAAGTGTAAAGCCTAATCGGCC

Name	Sequence
B C04 R11	AACCGCGGGGAGAGAATTACTATAAGAATAAACACC
B C05 R01	CCCTCAGAAGACTCCTCAAGAGAACTCATTAATATAAA
B C05 R02	CGCGAACGGCTTGAGGACTAAATCGGTTGGCAGAGGTGATGCAA
B C05 R03	TCCCCCTCACTATCATAACCTCGTGTGAATGCCATATGAGAAAA
B C05 R04	TAGGTAAAATAAGCCTCAGAGCTTCATATCACGCTTTCATCT
B C05 R05	GGATGTGCCTCAGGAAGATCGCACAATAGGAATGCGTTATAAACCG
B C06 R01	GCAGTCTCAAGTATTAAGAGGCTGACGCCAC
B C06 R02	CCTCAGAGTTAGTAATGAATTTGTTTCGA
B C06 R03	GGTGAATTAGCAACGGCTACAGAAAAGTACA
B C06 R04	ACGGAGATGACCTTCATCAAGAGTGCAGATT
B C06 R05	AAGAACTGGCATAGTAAGAGCAACAAATGCTT
B C06 R06	TAAACAGTGCAAACACTCCAACAGGTATTCCAA
B C06 R07	TTCTGCGAATTAGCAAATAAGCGATTCAA
B C06 R08	AGGGTGAGATCGTAAACTAGCATAAAATAAT
B C06 R09	TCGCGTCTCGACGACAGTATCGGCTGCAAGGC
B C06 R10	GATTAAGTCACAATTCCACACAACCGTATTGG
B C06 R11	GCGCCAGGGTGGTTTATAATCATCAGATGATGGCAA
B C07 R01	CTCATTATTCTGAAACATGATGAATTAGAGAAACA
B C07 R02	TCGCCTGGCATCGAACGAGGGCTTAAACGAATATACCAATTGAA
B C07 R03	CGAGAATAAAAGGAATTACGAGGCTCATTAATTGCGTGAACGTT
B C07 R04	GAGACAGCAGGCAAGGCAAAGAACGAGTAGAAATTATTATCAT
B C07 R05	GCCAGGGGCCAGTTGAGGGAGGCCATTCCAATAATGGGAAGGAGC
B C08 R01	TCATACATCTATTCTGGAACCTATTAGGGAT
B C08 R02	AGCAAGCCACGATCTAAAGTTTGACCGATA
B C08 R03	GTTGCGCTCAGCAGCGAAAGACAATAATTG
B C08 R04	TGTCAAAACGGTGTACAGACCAGCAGGACGT
B C08 R05	TGGGAAGAGCAGATAACATAACGCCGACCATAA
B C08 R06	ATCAAAAAAATTGAGCTTCAAAGTTGACCAT
B C08 R07	TAGATACACATCCAATAATCATATCAAATCA
B C08 R08	CCATCAATCTGGAGCAAACAAGAGAGCTTCA
B C08 R09	TCAACATTCTGTAACCGTCATTTTCCCA
B C08 R10	GTCACGACAGCTGTTCTGTGTGACCAGTGA
B C08 R11	GACGGGCAACAGCTGACGCCAGTGGTAATATCCAGAA
B C09 R01	ACCCATGTAGTTAATGCCCTCGGGCTTTGGAAAGCGT
B C09 R02	CTGCTCATGGGGATCGTCACCGACAATGACTGCCAATATAATCA
B C09 R03	TTACCCCTGACCACATTCAACTAATAAAATCTACAGTCAGTCCAT
B C09 R04	CAACCGTTATAGTAGTACGATTAATTGCAACTGAAATGTACTTCTT
B C09 R05	ACGACGGCGGTGTAGATGGCGAAAATGTGATGGAAATACTGAGTAG
B C10 R01	CTGGTAAAGTGGCCGTATAAACACCGTAAC
B C10 R02	ACTGAGTCATTCCACAGACAGCATGCCCA
B C10 R03	CGCATAAGTTAAAGGCCGCTTGTACTT
B C10 R04	AGCCGGAGAACTGACCAACTTAAACGAAC
B C10 R05	TAACGGATTGAGATTAGGAATACTATTAT
B C10 R06	AGTCAGAGAACGCCGAAAGACTTAACCTGT
B C10 R07	TTAGCTAGCATCAATTCTACTACTAGCTGA
B C10 R08	TAAATTATACAAAGGCTATCAGCAACCCGT
B C10 R09	CGGATTGGGATAGGTACGTTAGTGC
B C10 R10	AGCTTGCCTGACGAGCTCGAATCACCGCCT
B C10 R11	GGCCCTGAGAGAGTTCAGCAGGCGAAAATC
B C11 R01	CAGTGCCTGAGTAACTAAGTTGTATCA
B C11 R02	ACTACAACGCCCTGAGTTCGTCACCAAGTACAA
B C11 R03	CTGAGGCTTGCAGGGACCGATATACTGGACTCCAACGTC
B C11 R04	CAATCATAGGGAACACGAGGCGCAGACGGT

Name	Sequence
B C11 R05	TAGAAAGATTCATCAGACAACATTCACTTTGGAACAAGA
B C11 R06	TCAAAAAGATTAAGAGAGCAAAGCGGGATTGCA
B C11 R07	GCGAGCTGAAAAGGTGTATTTCAAGAATAGCCCGAGATA
B C11 R08	CTATTTTGAGAGATCATGCCGGAGAGGGTAG
B C11 R09	GCGGATTGACCGTAATTCCGTGGGCCAAATCGGAAAAT
B C11 R10	TCTAGAGGATCCCCGGATGCCTGCAGGTCGAC

4.2 Robot, track, cargo and goal strands

Table S2: Robot, track, cargo and goal strands.

Name	Sequence
robot	CCATTC CCTATCACACCATACTCTAC ATCCAC CCTCAAAACTTATCC ATCCAC
robot-Q	CCATTC CCTATCACACCATACTCTAC ATCCAC CCTCAAAACTTATCC ATCCAC /3IAbRQSp/
robot inhibitor	GTGCTC GTGGAT GTAGAGTATGGTGTGATAGG GAATGG
robot trigger	CCTATCACACCATACTCTAC ATCCAC GAGCAC
robot start attacher	GGAAAGTAAGTAGAAG GTGGAT GGATAAGTTTGAGG
robot start staple	CTTCTACTTACTTCC TT - staple
track1 staple	staple - TTTT GTGGAT GGATAAGTTTGAGG
track2 staple	staple - TTTTT GGATAAGTTTGAGG GTGGAT
robot goal staple	staple - TTTTT GTGGAT GGATAAGTTTGAGG GTGGAT
cargo1	AGATGT GTAGAGTATGGTGTGATAGG GAATGG TT
cargo1-F	AGATGT GTAGAGTATGGTGTGATAGG GAATGG TT /3ATTO532N/
cargo1 attacher	CCTATCACACCATACTCTAC ACCTTACCTCATCCCTAACTT
cargo1 attacher-Q	/5IAbRQ/ CCTATCACACCATACTCTAC ACCTTACCTCATCCCTAACTT
cargo1 staple	staple - TTTT AAGTTAGGGATGAGGTAAAGGT
cargo2	GAAAGG GTAGAGTATGGTGTGATAGG GAATGG TT
cargo2-F	GAAAGG GTAGAGTATGGTGTGATAGG GAATGG TT /3ATTO590N/
cargo2 attacher	CCTATCACACCATACTCTAC CTCCCTACCCATATCACCTT
cargo2 attacher-Q	/5IAbRQ/ CCTATCACACCATACTCTAC CTCCCTACCCATATCACCTT
cargo2 staple	staple - TTTT AAGGTGATATGGTAGGGAG
goal1	CCATTC CCTATCACACCATACTCTAC ACATCT ACTAACTCCTACCCACACCT
goal1-Q	/5IAbRQ/ CCATTC CCTATCACACCATACTCTAC ACATCT ACTAACTCCTACCCACACCT
goal1 staple	staple - TTTT AGGTGTGGTAGGAGTTAGT
goal2	CCATTC CCTATCACACCATACTCTAC CCTTTC CAACTCTCCACTCCAATCAA
goal2-Q	/5IAbRQ/ CCATTC CCTATCACACCATACTCTAC CCTTTC CAACTCTCCACTCCAATCAA
goal2 staple	stape - TTTT TTGATTGGAGTGGAGAGTTG
goal1 inhibitor	AGATGT GTAGAGTATG ACACCTT
goal2 inhibitor	GAAAGG GTAGAGTATG ACACCTT
goal inhibitor	ACTCTA GTGTGATAGG GAATGG
goal trigger1	AAGTGT CATACTCTAC
goal trigger2	CCTATCACAC TAGAGT

References

1. Mark Yim, Wei-Min Shen, Behnam Salemi, Daniela Rus, Mark Moll, Hod Lipson, Eric Klavins, and Gregory S Chirikjian. Modular self-reconfigurable robot systems [grand challenges of robotics]. *IEEE Robotics & Automation Magazine*, 14(1):43–52, 2007.
2. Muneaki Nakamura, Lu Chen, Stuart C Howes, Tony D Schindler, Eva Nogales, and Zev Bryant. Remote control of myosin and kinesin motors using light-activated gearshifting. *Nature Nanotechnology*, 9(9):693–697, 2014.
3. Akane Furuta, Misako Amino, Maki Yoshio, Kazuhiro Oiwa, Hiroaki Kojima, and Ken’ya Furuta. Creating biomolecular motors based on dynein and actin-binding proteins. *Nature Nanotechnology*, 12(3):233–237, 2017.
4. Turlough Neary and Damien Woods. The complexity of small universal Turing machines: a survey. In *SOFSEM: Theory and Practice of Computer Science*, volume 7147 of *LNCS*, pages 385–405. Springer, 2012.
5. Eric Bonabeau, Marco Dorigo, and Guy Theraulaz. Inspiration for optimization from social insect behaviour. *Nature*, 406(6791):39–42, 2000.
6. Paul WK Rothemund. Folding DNA to create nanoscale shapes and patterns. *Nature*, 440(7082):297–302, 2006.
7. Nadrian C Seeman. Nucleic acid junctions and lattices. *Journal of Theoretical Biology*, 99(2):237–247, 1982.
8. Bernard Yurke, Andrew J Turberfield, Allen P Mills, Friedrich C Simmel, and Jennifer L Neumann. A DNA-fuelled molecular machine made of dna. *Nature*, 406(6796):605–608, 2000.
9. Suvir Venkataraman, Robert M Dirks, Paul WK Rothemund, Erik Winfree, and Niles A Pierce. An autonomous polymerization motor powered by DNA hybridization. *Nature Nanotechnology*, 2(8):490–494, 2007.
10. Philip Ketterer, Elena M Willner, and Hendrik Dietz. Nanoscale rotary apparatus formed from tight-fitting 3D DNA components. *Science Advances*, 2(2):e1501209, 2016.
11. William B Sherman and Nadrian C Seeman. A precisely controlled DNA biped walking device. *Nano Letters*, 4(7):1203–1207, 2004.
12. Jong-Shik Shin and Niles A Pierce. A synthetic DNA walker for molecular transport. *Journal of the American Chemical Society*, 126(35):10834–10835, 2004.
13. Peng Yin, Hao Yan, Xiaoju G Daniell, Andrew J Turberfield, and John H Reif. A unidirectional DNA walker that moves autonomously along a track. *Angewandte Chemie International Edition*, 43(37):4906–4911, 2004.
14. Jonathan Bath, Simon J Green, and Andrew J Turberfield. A free-running DNA motor powered by a nicking enzyme. *Angewandte Chemie International Edition*, 117(28):4432–4435, 2005.

15. Ye Tian, Yu He, Yi Chen, Peng Yin, and Chengde Mao. A DNAzyme that walks processively and autonomously along a one-dimensional track. *Angewandte Chemie International Edition*, 44(28):4355–4358, 2005.
16. Renjun Pei, Steven K Taylor, Darko Stefanovic, Sergei Rudchenko, Tiffany E Mitchell, and Milan N Stojanovic. Behavior of polycatalytic assemblies in a substrate-displaying matrix. *Journal of the American Chemical Society*, 128(39):12693–12699, 2006.
17. Peng Yin, Harry MT Choi, Colby R Calvert, and Niles A Pierce. Programming biomolecular self-assembly pathways. *Nature*, 451(7176):318–322, 2008.
18. Tosan Omabegho, Ruojie Sha, and Nadrian C Seeman. A bipedal DNA brownian motor with coordinated legs. *Science*, 324(5923):67–71, 2009.
19. Kyle Lund, Anthony J Manzo, Nadine Dabby, Nicole Michelotti, Alexander Johnson-Buck, Jeanette Nangreave, Steven Taylor, Renjun Pei, Milan N Stojanovic, Nils G Walter, et al. Molecular robots guided by prescriptive landscapes. *Nature*, 465(7295):206–210, 2010.
20. Shelley FJ Wickham, Jonathan Bath, Yousuke Katsuda, Masayuki Endo, Kumi Hidaka, Hiroshi Sugiyama, and Andrew J Turberfield. A DNA-based molecular motor that can navigate a network of tracks. *Nature Nanotechnology*, 7(3):169–173, 2012.
21. Hongzhou Gu, Jie Chao, Shou-Jun Xiao, and Nadrian C Seeman. A proximity-based programmable DNA nanoscale assembly line. *Nature*, 465(7295):202–205, 2010.
22. C Jung, PB Allen, and AD Ellington. A stochastic DNA walker that traverses a microparticle surface. *Nature Nanotechnology*, 11(2):157–163, 2016.
23. Marvin Bentley and Gary Bunker. The cellular mechanisms that maintain neuronal polarity. *Nature Reviews Neuroscience*, 17(10):611–622, 2016.
24. Nigel R Franks and Ana B Sendova-Franks. Brood sorting by ants: distributing the workload over the work-surface. *Behavioral Ecology and Sociobiology*, 30(2):109–123, 1992.
25. Donald Ervin Knuth. *The art of computer programming: sorting and searching*, volume 3. Pearson Education, 1998.
26. Spyros Artavanis-Tsakonas, Matthew D Rand, and Robert J Lake. Notch signaling: cell fate control and signal integration in development. *Science*, 284(5415):770–776, 1999.
27. Jean-Louis Deneubourg, Simon Goss, Nigel Franks, Ana Sendova-Franks, Claire Detrain, and Laetitia Chrétien. The dynamics of collective sorting robot-like ants and ant-like robots. In *Proceedings of the first international conference on simulation of adaptive behavior on From animals to animats*, pages 356–363, 1991.
28. Owen Holland and Chris Melhuish. Stigmergy, self-organization, and sorting in collective robotics. *Artificial Life*, 5(2):173–202, 1999.
29. Andrew J Turberfield, JC Mitchell, Bernard Yurke, Allen P Mills Jr, MI Blakey, and Friedrich C Simmel. DNA fuel for free-running nanomachines. *Physical Review Letters*, 90(11):118102, 2003.

30. David Yu Zhang and Erik Winfree. Control of DNA strand displacement kinetics using toehold exchange. *Journal of the American Chemical Society*, 131(47):17303–17314, 2009.
31. László Lovász. Random walks on graphs: a survey. *Combinatorics*, 2:1–46, 1993.
32. Carlos Ernesto Castro, Fabian Kilchherr, Do-Nyun Kim, Enrique Lin Shiao, Tobias Wauer, Philipp Wortmann, Mark Bathe, and Hendrik Dietz. A primer to scaffolded DNA origami. *Nature Methods*, 8(3):221–229, 2011.
33. Petr Šulc, Thomas E Ouldridge, Flavio Romano, Jonathan PK Doye, and Ard A Louis. Simulating a burnt-bridges DNA motor with a coarse-grained DNA model. *Natural Computing*, 13(4):535–547, 2014.
34. Steven B Smith, Yujia Cui, and Carlos Bustamante. Overstretching B-DNA: the elastic response of individual double-stranded and single-stranded DNA molecules. *Science*, 271(5250):795–799, 1996.
35. Shelley FJ Wickham, Masayuki Endo, Yousuke Katsuda, Kumi Hidaka, Jonathan Bath, Hiroshi Sugiyama, and Andrew J Turberfield. Direct observation of stepwise movement of a synthetic molecular transporter. *Nature Nanotechnology*, 6(3):166–169, 2011.
36. Alexander Johnson-Buck, Jeanette Nangreave, Shuxing Jiang, Hao Yan, and Nils G Walter. Multifactorial modulation of binding and dissociation kinetics on two-dimensional DNA nanostructures. *Nano Letters*, 13(6):2754–2759, 2013.
37. Mario Teichmann, Enzo Kopperger, and Friedrich C Simmel. Robustness of localized DNA strand displacement cascades. *ACS Nano*, 8(8):8487–8496, 2014.
38. Nobutaka Hirokawa, Yasuko Noda, Yosuke Tanaka, and Shinsuke Niwa. Kinesin superfamily motor proteins and intracellular transport. *Nature Reviews Molecular Cell Biology*, 10(10):682–696, 2009.
39. Kevin Yehl, Andrew Mugler, Skanda Vivek, Yang Liu, Yun Zhang, Mengzhen Fan, Eric R Weeks, and Khalid Salaita. High-speed DNA-based rolling motors powered by RNase H. *Nature Nanotechnology*, 11(2):184–190, 2016.
40. Adam JM Wollman, Carlos Sanchez-Cano, Helen MJ Carstairs, Robert A Cross, and Andrew J Turberfield. Transport and self-organization across different length scales powered by motor proteins and programmed by DNA. *Nature Nanotechnology*, 9(1):44–47, 2014.
41. Grigory Tikhomirov, Philip Petersen, and Lulu Qian. Programmable disorder in random DNA tilings. *Nature Nanotechnology*, 12(3):251–259, 2017.
42. Richard A Muscat, Jonathan Bath, and Andrew J Turberfield. Small molecule signals that direct the route of a molecular cargo. *Small*, 8(23):3593–3597, 2012.
43. Yu He and David R Liu. Autonomous multistep organic synthesis in a single isothermal solution mediated by a DNA walker. *Nature Nanotechnology*, 5(11):778–782, 2010.
44. Wenjing Meng, Richard A Muscat, Mireya L McKee, Phillip J Milnes, Afaf H El-Sagheer, Jonathan Bath, Benjamin G Davis, Tom Brown, Rachel K O'Reilly, and Andrew J Turberfield. An autonomous molecular assembler for programmable chemical synthesis. *Nature Chemistry*, 8(6):542–548, 2016.

45. Tae-Gon Cha, Jing Pan, Haorong Chen, Janette Salgado, Xiang Li, Chengde Mao, and Jong Hyun Choi. A synthetic DNA motor that transports nanoparticles along carbon nanotubes. *Nature Nanotechnology*, 9(1):39–43, 2014.
46. Anton Kuzyk, Yangyang Yang, Xiaoyang Duan, Simon Stoll, Alexander O Govorov, Hiroshi Sugiyama, Masayuki Endo, and Na Liu. A light-driven three-dimensional plasmonic nanosystem that translates molecular motion into reversible chiroptical function. *Nature Communications*, 7, 2016.
47. Shawn M Douglas, Ido Bachelet, and George M Church. A logic-gated nanorobot for targeted transport of molecular payloads. *Science*, 335(6070):831–834, 2012.
48. Hanyong Peng, Xing-Fang Li, Hongquan Zhang, and X Chris Le. A microRNA-initiated DNAAzyme motor operating in living cells. *Nature Communications*, 8, 2017.
49. Michael Rubenstein, Alejandro Cornejo, and Radhika Nagpal. Programmable self-assembly in a thousand-robot swarm. *Science*, 345(6198):795–799, 2014.
50. Gourab Chatterjee, Neil Dalchau, Richard A Muscat, Andrew Phillips, and Georg Seelig. A spatially localized architecture for fast and modular DNA computing. *Nature Nanotechnology*, 2017. doi:10.1038/nnano.2017.127.
51. Lulu Qian and Erik Winfree. Parallel and scalable computation and spatial dynamics with DNA-based chemical reaction networks on a surface. *Lecture Notes in Computer Science*, 8727:114–131, 2014.
52. Joseph N Zadeh, Conrad D Steenberg, Justin S Bois, Brian R Wolfe, Marshall B Pierce, Asif R Khan, Robert M Dirks, and Niles A Pierce. NUPACK: analysis and design of nucleic acid systems. *Journal of Computational Chemistry*, 32(1):170–173, 2011.
53. Neil Dalchau, Harish Chandran, Nikhil Gopalkrishnan, Andrew Phillips, and John Reif. Probabilistic analysis of localized DNA hybridization circuits. *ACS Synthetic Biology*, 4(8):898–913, 2015.
54. James G Wetmur. Hybridization and renaturation kinetics of nucleic acids. *Annual Review of Biophysics and Bioengineering*, 5(1):337–361, 1976.
55. Grégoire Bonnet, Oleg Krichevsky, and Albert Libchaber. Kinetics of conformational fluctuations in DNA hairpin-loops. *Proceedings of the National Academy of Sciences*, 95(15):8602–8606, 1998.
56. Niranjan Srinivas, Thomas E Ouldridge, Petr Šulc, Joseph M Schaeffer, Bernard Yurke, Ard A Louis, Jonathan PK Doye, and Erik Winfree. On the biophysics and kinetics of toehold-mediated DNA strand displacement. *Nucleic Acids Research*, 41(22):10641–10658, 2013.
57. Sidney Redner. *A guide to first-passage processes*. Cambridge University Press, 2001.